Journal of Asian Earth Sciences 231 (2022) 105221

Contents lists available at ScienceDirect

Journal of Asian Earth Sciences

journal homepage: www.elsevier.com/locate/jseaes

Conventional and unconventional petroleum potentials of the Late Jurassic Madbi organic-rich shales from the Sunah oilfield in the Say'un–Masilah Basin, Eastern Yemen

Mohammed Hail Hakimi [a,*], Mikhail A. Varfolomeev [b], Ali Y. Kahal [c], Abbas F. Gharib [d], Fahad Alshehri [c], Afikah Rahim [e], Hussain J. Al Faifi [c], Ameen A. Al-Muntaser [b], Saleh Qaysi [c], Karem Abdelmohsen [f]

[a] Geology Department, Faculty of Applied Science, Taiz University, 6803 Taiz, Yemen
[b] Department of Petroleum Engineering, Kazan Federal University, Kazan 420008, Russia
[c] Geology and Geophysics Department, College of Science, King Saud University, Riyadh, Saudi Arabia
[d] Department of Oil and Gas Economics, College of Administrative and Financial Science, Imam Ja'afar Al-Sadiq University, Baghdad, Iraq
[e] School of Civil Engineering, Faculty of Engineering, Universiti Teknologi Malaysia, Johor, Malaysia
[f] Department of Geological and Environmental Sciences, Western Michigan University, Kalamazoo, MI 49008, USA

ARTICLE INFO

Keywords:
Madbi formation
Basin modeling
Conventional and unconventional oil potentials
Sunah oilfield
Sayun–Masilah Basin
Yemen

ABSTRACT

This study aims to carry out the detailed geochemical characterization of the Madbi organic-rich shale intervals from structural heights in the Sunah oilfield, Say'un–Masilah Basin. The geochemical and basin model results of the source rock reveal that the Madbi Formation in the Sunah oilfield have both conventional and unconventional oil resource potential, and can laterally and vertically change from one well site to another due to varying burial temperature distributions with increasing depth. The Madbi source rock from structural heights of the oilfield is characterized by high organic content, with total organic matter (TOC) values of up to 12 wt%, and reached the low mature stage of the oil generation window. These characteristics make them a potential yet unconventional oil resource candidate, resulting in the retention of more oil that could be released upon application of similarly unconventional techniques. The conventional petroleum system of the Madbi Formation in the deeper portions in the Sunah oilfield was identified based on the match between source, reservoir and seal rocks, and timing of generation, migration, trap formation, and preservation. This Madbi source rock set reached relatively high maturity in the peak-oil window, with ratios of approximately 10–50% of the kerogen converted to large amounts of oil since the late Eocene-early Oligocene. To date, the conversion ratios of kerogen have reached their highest values of more than 50%, generating significant amounts of oil and leading to high pressures and subsequent oil expulsion, which reached the trapping site via vertical migration paths through the faults.

1. Introduction

The recent rise in the fuel demand from automobile and other linked industries have increased conventional petroleum production using established sources and reservoir rocks around the globe (Qadri et al., 2021). However, the quality of the increased production of conventional reserves has declined. This decrease in conventional petroleum has also forced innovations in hydrocarbon geared towards more discoveries and re-evaluations of already discovered petroleum source rocks as unconventional petroleum resources. Understanding the potential of conventional and unconventional resources is a significant research subject in geology, particularly petroleum geology, and it is important for hydrocarbon generation, shale reservoir quality, paleoenvironmental reconstruction, mineral deposition, and oil and gas distribution (Caineng et al., 2013; Wu et al., 2019; Qadri et al., 2016).

Petroleum geology is evolving into two branches, conventional and unconventional petroleum geology, with the latter becoming a new frontier in the petroleum industry. On the one hand, identifying the

* Corresponding author.
E-mail address: ibnalhakimi@taiz.edu.ye (M.H. Hakimi).

https://doi.org/10.1016/j.jseaes.2022.105221
Received 31 October 2021; Received in revised form 4 April 2022; Accepted 5 April 2022
Available online 8 April 2022

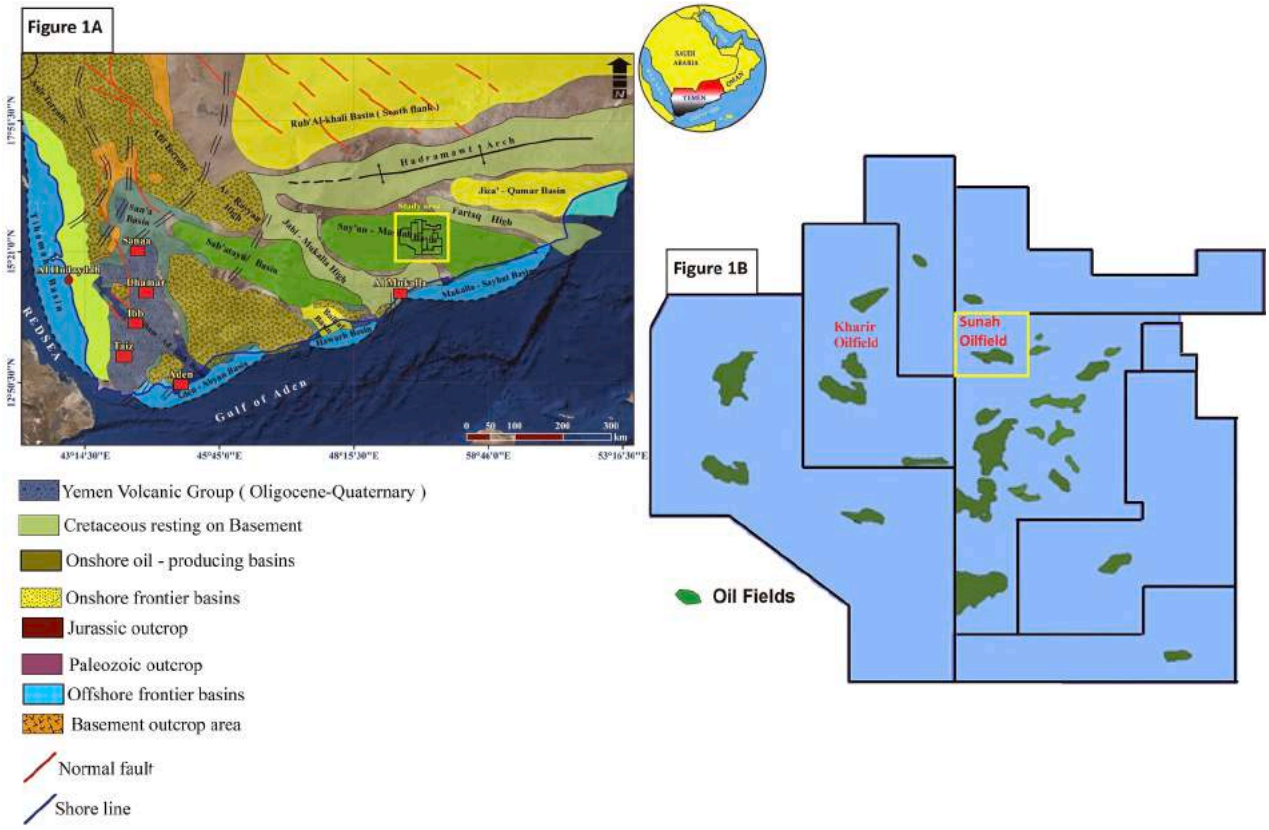

Fig. 1. (A) Map of the main onshore Sab'atayn, Say'un–Masilah, Balhaf and Jiza-Qamar basins and offshore basins along the Gulf of Aden and the Red Sea, including Aden-Abyan, Hawarh, Mukalla-Sayhut and Tihamah basins (modified after As-Saruri et al., 2010), including study area (yellow square), and (B) main producing oilfields in the Central portion of Say'un –Masilah Basin, including Sunah Oilfield. (For interpretation of the references to color in this figure legend, the reader is referred to the web version of this article.)

match between the source rock, reservoir, seal rock, timing of generation migration, and trap formation is the main aim of conventional petroleum geological study (Caineng et al., 2013; Qadri et al., 2016; Radwan et al., 2021). However, the study of unconventional hydrocarbon resources is based on evaluating the lithology, physical properties, brittleness, oiliness, source rock features, and accumulations of oil and gas at various fine-grain sediments, focusing on shale and carbonate, with low limits of pore throat diameter (Caineng et al., 2013; Boutaleb et al., 2021).

In the petroleum industry, it is important to understand the various geochemical processes, basin modeling history, and source rock characteristics in order to retrieve the potential of conventional and unconventional resources and enable hydrocarbon exploitation (Caineng et al., 2013). In turn, the integration of sedimentological, geochemical characteristics, basin modeling, and tectonic style or geological history by applying various techniques has significantly informed both conventional and unconventional resource exploitation. For instance, the tectonic system plays an important role in the distribution of temperatures across the sedimentary basins by forming lows and highs with different formation temperatures (Lachenbruch, 1970; Allen and Allen, 1990).

The Say'un–Masilah Basin, which is the subject of this research, is classified as one of Yemen's major oil-producing basins, containing many fields of commercial quantities of oil, including the Sunah oilfield (Fig. 1B). However, the Say'un–Masilah Basin has excellent source rocks for petroleum exploration that include organic-rich carbonate and subordinate shale within the Late Jurassic–Early Cretaceous successions such as the formations of Madbi, Nayfa, and Saar (e.g., Hakimi et al., 2010; Al-Areeq, 2018; Hakimi et al., 2020a, 2020b). The organic-rich intervals within the Late Jurassic Madbi Formation and their characteristics and capacity for hydrocarbon generation potential have received unprecedented attention from numerous scientific researchers (e.g., Hakimi et al., 2010; Al-Areeq, 2018). Biomarker fingerprints of reservoir oils in the basin were also investigated, and it was widely documented that the mature Madbi source rock is directly linked with the main petroleum-producing areas identified to date, which act as a conventional petroleum resource (e.g., Hakimi et al., 2011; Al Areeq and Maky, 2015). This mature source rock of the Madbi Formation was mainly located in the flanks of the basin, where it reached a high maturation level and readily yielded oil in the kitchen areas (Hakimi et al., 2010).

Following the previous studies, the current study intends to expand existing knowledge on the conventional and unconventional resources for further petroleum exploration in the basin by characterizing the organic matter along with the oil generation resource of the Madbi organic-rich shales from the structural heights in the Say'un–Masilah Basin. Moreover, the oil generation and expulsion over time from the Madbi source rock were numerically simulated and used to assess the genetic connection and outline the potential of the conventional and unconventional oil resources.

2. Geological background

Yemen has been divided into three rift-generating tectonic systems, two of which occurred during the Mesozoic Era and one during the Cenozoic Era, and are generally bounded by major faults (Redfern and Jones, 1995; Beydoun et al., 1996; As-Saruri et al., 2010). This extensional tectonics system related to Mesozoic and Cenozoic phases of rifting has resulted in petroleum structural traps in all the rift basins in Yemen, including fault-bounded horst blocks and tilted blocks (Al-Johi

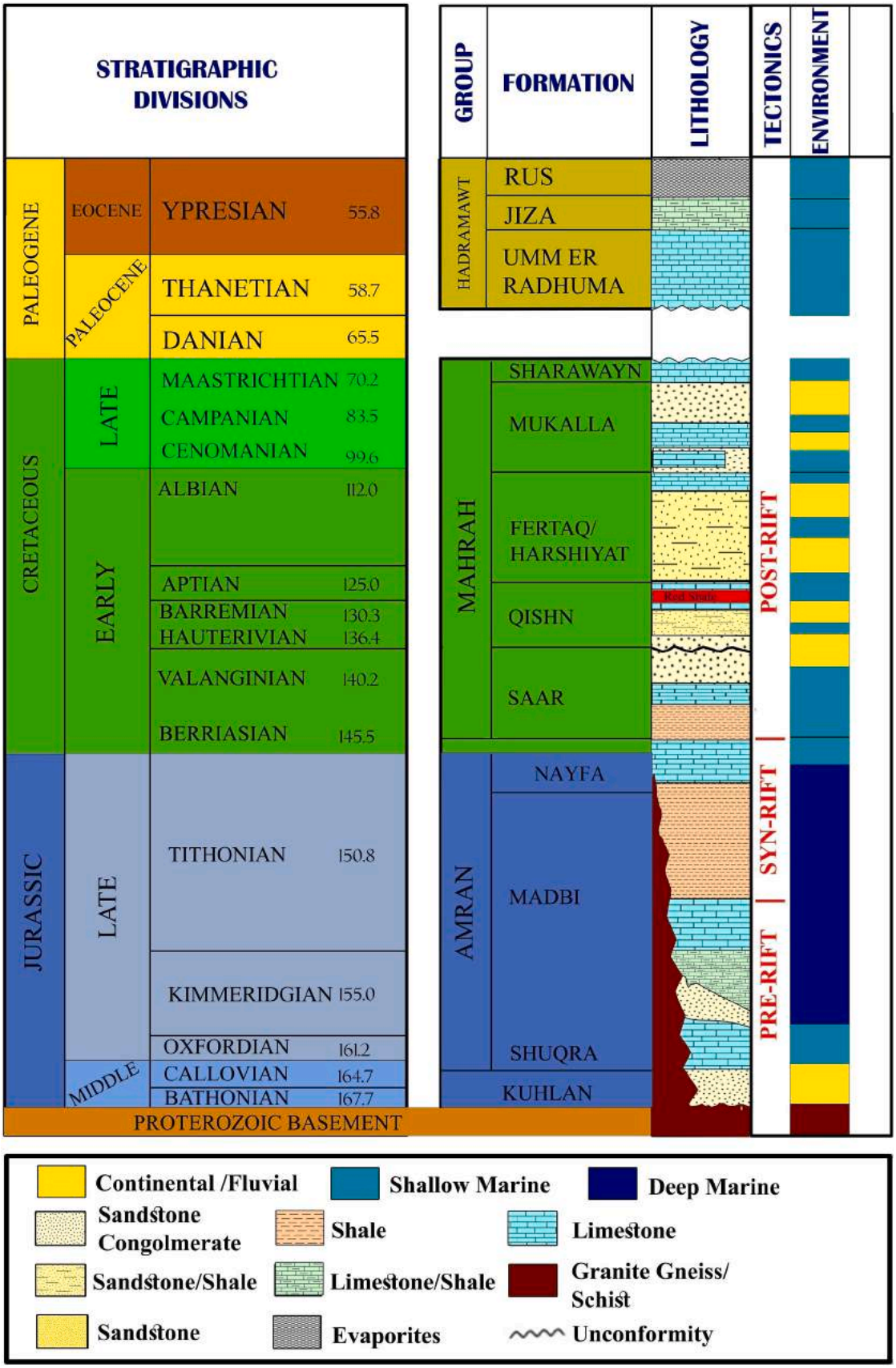

Fig. 2. Generalized stratigraphic column of a thick Mesozoic succession (Jurassic-Cretaceous) followed by a Paleogene succession (Paleocene-Eocene) in the Say'un-Masilah Basin (modified after Al-Johi et al., 2019).

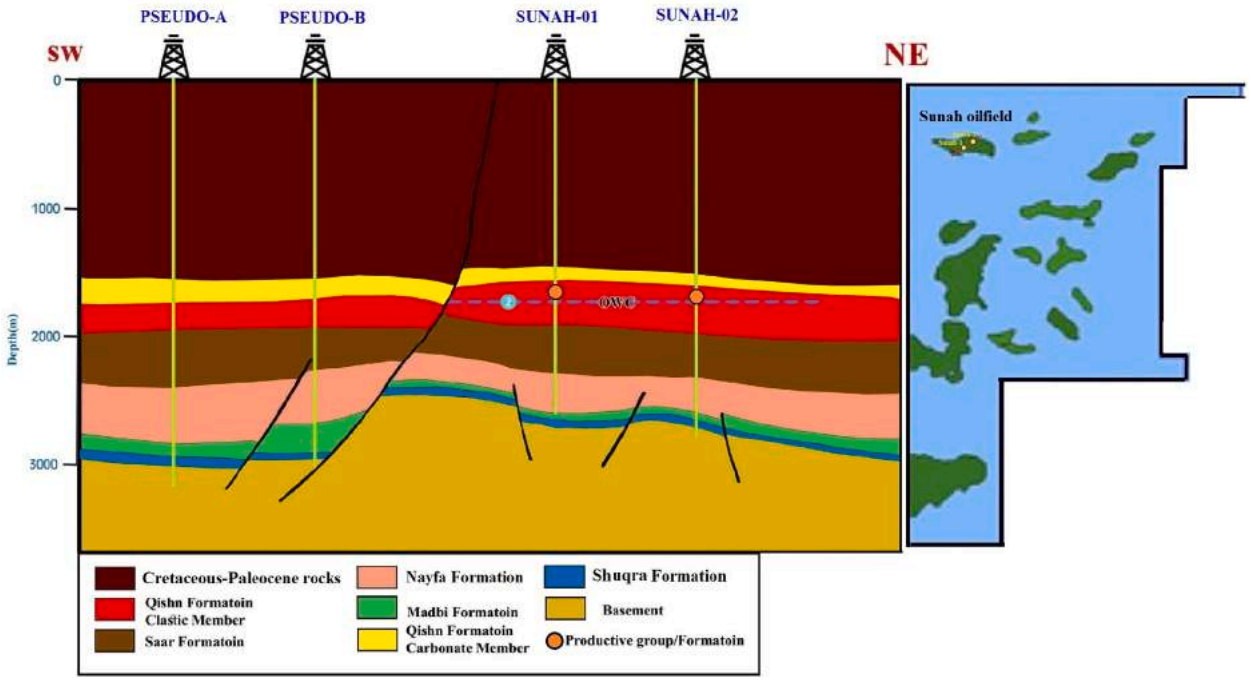

Fig. 3. Schematic geological cross section across the Sunah Oilfield, including four well locations, showing the primary structural setting and stratigraphic succession, including Madbi source rock (modified after SPT, 1994).

et al., 2019).

The continental Sab'atayn and Say'un–Masilah rift basins (Fig. 1A) were initially formed in the early Kimmeridgian and continued rifting till the earliest part of the Cretaceous (Redfern and Jones, 1995; Beydoun et al., 1996; As-Saruri et al., 2010). A second episode of rifting resulted in basins to the east (Balhaf and Jiza-Qamar Basins, Fig. 1A) that, with the further extension of the earlier Sab'atayn and Say'un–Masilah basins, are due to the separation of the Afro-Arabian Plate from that of Madagascar-India (Mountain and Prell, 1990). During the post-Eocene to Miocene, active rifting occurred in the western and southern parts of Yemen, forming the Aden-Abyan, Hawarh, and Mukalla-Sayhut Basins in the south and Tihamah Basin in western Yemen (Fig. 1A). Cenozoic rifting is ultimately related to the opening of the Red Sea and Gulf of Aden oceanic basins, essentially propagating from east to west along the Gulf of Aden and south to north along the Red Sea (Haitham, and Nani, 1990; Redfern and Jones, 1995; Bosworth et al., 2005).

The generalized stratigraphic succession in the sedimentary section of Yemen, including the Say'un–Masilah Basin, has been studied and identified by several researchers such as Beydoun et al. (1998) and As-Saruri et al. (2010). These scholars concluded that the sedimentary section contains thick Mesozoic and Cenozoic rocks (Fig. 2). Important regional unconformities related to tectonic and/or erosion events have also been indicated (e.g., Beydoun et al., 1998; As-Saruri et al., 2010). The sequences are divided into pre-rift, *syn*-rift, and post-rift stages (Fig. 2). However, detailed reviews and analyses of sedimentologic with stratigraphic and tectonic properties of the Say'un–Masilah Basin and basin-fill architecture are summarized and can be obtained from numerous literature (e.g., Beydoun et al., 1998; As-Saruri et al., 2010; Al-Johi et al., 2019).

The Madbi Formation, which is the focus of this study, is widespread and present in the majority of Mesozoic rift basins in Yemen (As-Saruri et al., 2010). The Madbi Formation was deposited in the Late Jurassic (Kimmeridgian–Tithonian) during the main phase of rifting (Brannin et al., 1999; As-Saruri et al., 2010), consisting of a variety of lithologies from shallow to relatively deep marine limestone, shallow marine sandstones, and organically rich shales (Fig. 2). The organic-rich shales within the Madbi Formation are reported to be oil-bearing in most oilfields of the Say'un–Masilah Basin (e.g., Al-Areeq et al., 2020; Hakimi et al., 2010).

In most of the subsurface wells, the Madbi Formation is conformably overlain by the late Tithonian–early Berriasian Nayfa Formation (Fig. 2). The Nayfa Formation is slightly similar in lithology to the underlying Madbi Formation described above, indicating the relatively continuous deep water and *syn*-rift conditions. However, the Nayfa Formation comprises more carbonate rocks with subordinate shales (Fig. 2). The formation is thus equivalent in age to the shallow marine carbonates that occur within the Kahmah Group in Oman (Hughes Clarke, 1988). However, the sediments of the Nayfa Formation were followed by thick clastic and carbonate successions of the Saar and younger formations with intermittent hiatuses (Fig. 2), resulting from Cretaceous tectonic and eustatic fluctuations.

3. Materials and methods

3.1. Sampling and geochemical analyses

Twenty-four core, side well core, and cutting samples of the Jurassic Madbi organic-rich shale intervals were collected from the Sunah-1 well, Sunah oilfield (Fig. 1B). These organic-rich shale samples reached shallower depths of 2500–2600 m (Table 1). In addition, three oil samples incurred from reservoir rocks represented in the same well (Sunah-1) were also geochemically analyzed.

Source rock geochemical analyses were performed on the collected Madbi shale samples, including total organic carbon (TOC) content, Rock-Eval (RE) pyrolysis, and bitumen extraction. The TOC estimation and RE pyrolysis techniques were conducted using about 100 mg powder analyzed samples via LECO CS-125 and RE II instruments, respectively.

The RE analysis was used as a screening method, and several parameters were measured, including S_1 (free bitumen), S_2 (amount of petroleum generated by thermal alteration of insoluble kerogen), S_3 (quantity of CO_2 released by cracking of kerogen), and T_{max} (maximum temperature of S_2 yield), as shown in Table 1. The other geochemical

Table 1
Geochemical results of the analyzed organic-rich shale samples within the Late Jurassic Madbi Formation from one shallow well location (Sunah-1) in the Sunah Oilfield, Central portion of Say'un-Masilah Basin, including TOC content and Rock-Eval pyrolysis.

Field	Well	Sample type	Depth (m)	TOC Wt. %	Rock-Eval pyrolysis data							
					S_1-HC (mg/g)	S_2-HC (mg/g)	S_3-CO_2 (mg/g)	HI (mg/g)	OI (mg/g)	S_2/S_1 (mg/g)	PI (mg/g)	T_{max} (°C)
Sunah Oilfield	Sunah-1	Cutting	2585.0	5.69								
		Core	2585.0	8.37	5.6	49.55	0.75	592	9	65.78	0.10	443
		Core	2585.0	12.60	7.9	70.43	0.50	559	4	139.75	0.10	443
		Side well core	2586.4	6.10	7.0	33.86	0.61	555	10	55.50	0.17	442
		Side well core	2587.0	4.07	4.5	20.15	0.45	495	11	45.00	0.18	439
		Side well core	2588.0	8.16	6.5	43.57	0.57	534	7	76.29	0.13	441
		Side well core	2589.0	11.80	7.5	66.32	0.47	562	4	140.50	0.10	442
		Side well core	2590.0	6.85	5.1	40.21	0.34	587	5	117.40	0.11	441
		Cutting	2591.0	6.75								
		Core	2591.0	7.90	4.9	41.55	0.87	526	11	47.82	0.11	443
		Core	2591.0	11.00	8.1	63.25	0.99	575	9	63.89	0.11	442
		Side well core	2591.3	8.82	5.1	54.07	0.35	613	4	153.25	0.09	438
		Side well core	2592.7	2.75	3.2	12.65	0.55	460	20	23.00	0.20	437
		Side well core	2593.4	3.48	3.9	17.02	0.38	489	11	44.45	0.19	432
		Cutting	2595.0	4.94								
		Core	2595.0	7.37	5.5	42.60	0.66	578	9	64.22	0.11	442
		Core	2595.0	7.41	5.6	40.38	0.82	545	11	49.55	0.12	441
		Side well core	2598.5	5.92	5.8	31.49	0.65	532	11	48.36	0.16	442
		Side well core	2602.0	4.63	4.1	23.29	0.51	503	11	45.73	0.15	444
		Cutting	2605.0	4.15								
		Core	2605.0	4.08	3.3	20.44	0.49	501	12	41.75	0.14	440
		Core	2605.0	5.96	4.4	31.71	0.24	532	4	133.00	0.12	442
		Side well core	2606.5	4.00	4.5	17.24	0.64	431	16	26.94	0.21	439
		Side well core	2610.7	4.05	4.3	22.44	0.53	554	13	42.62	0.16	440

TOC = Total Organic Carbon; S_1-peak = Free contents of hydrocarbon(mg HC/g rock); S_2-peak = Remaining hydrocarbon potential (mg HC/g rock); S_3-peak = Produced carbon dioxide (mg CO_2/g rock); HI = $S_2 \times 100$/TOC(mg HC/g rock); OI = $S_3 \times 100$/TOC (mg CO_2/g TOC); T_{max} = Maximum temperature at peak of S_2(°C); PI = Production index [$S_1/(S_1 + S_2)$]

parameters like hydrogen index (HI), oxygen index (OI), and production index (PI) were calculated as explained by previous researchers (e.g., Peters and Cassa, 1994) and presented in Table 1.

The bitumen was further extracted from seven shale rock samples using mixed solvents of dichloromethane and methanol (93:7 v/v) for duration of about 72 h. The extracted bitumen from the shale rock samples and whole crude oils was fractionated into saturated and aromatic hydrocarbons and polar using liquid column chromatography with petroleum ether, dichloromethane, and methanol solvents, respectively.

The saturated fraction of the seven extracted rocks and three oils were subsequently analyzed using a flame ionization detector (FID) of a gas chromatograph (GC). The GC was connected using an AMS 92 column under temperatures programmed between 70 °C and 270 °C at a gradual increment rate of 25 °C/min and then kept at 290 °C for 20 min.

In addition, the saturated and aromatic hydrocarbon fractions of the two extracted rock samples and two oils were tested by gas chromatography–mass spectrometry (GC–MS) using the Finnegan 4000 mass spectrometer. The programmed temperature of the GC–MS was gradually increased from 60 °C to 300 °C at a rate of 25 °C/min and then held at 300 °C for 20 min at the end of the procedure. The GC–MS technique was implemented to identify the lipid biomarkers (i.e., isoprenoids, terpenes, triterpenes, steranes, and diasteranes) in the aliphatic hydrocarbon (HC) fraction using specific ions such as *m/z* 191 and *m/z* 217 mass fragmentograms.

For the aromatic biomarkers, several parameters and ratios, such as methyl phenanthrene (MPI) and dibenzothiophene/phenanthrene (DBT/P), were identified and calculated from the combination of ions *m/z* 178, 184, and 192. The saturated and aromatic biomarkers were identified from the retention times together with mass spectra as previously reported (e.g., Radke et al., 1986; Makeen et al., 2015; Hakimi et al., 2011), and their ratios and parameters were estimated by measurement using heights of peaks as shown in Table 3.

For the stable carbon isotope ($^{\delta 13}C$; in VPDB), the saturated and aromatic fractions from the three extracted rocks and three oils were also analyzed using a VG 602 stable isotope mass spectrometry instrument to outline the genetic link between the oils and their probable source rocks.

American Petroleum Institute (API) gravity and analysis of inorganic geochemical elements including sulfur, nickel (Ni), and vanadium (V) were further conducted on three investigated oil samples. The American Petroleum Institute (API) gravity of the whole crude oils was measured via the IP60 method, and the inorganic elements of sulfur content (wt %), nickel (ppm), and vanadium (ppm) were also measured using inductively coupled plasma (ICP).

3.2. Vitrinite reflectance analysis

For this study, the vitrinite reflectance (%VRo) analysis was performed on twenty-two (22) samples through geological formations in the Sunah-1 well, including the Madbi Formation (Table 4). The 22

Table 2
Geochemical and physical characteristics of the analyzed seven representative organic-rich shale samples of the Madbi Formation and three oil samples from the clastic and carbonate reservoir rock in the Sunah Oilfield, Central portion of Say'un-Masilah Basin, including American Petroleum Institute (API), sulfur content (S), Nickel (Ni), Vanadium (V), bulk oil composition (i.e. saturated, aromatic, NSO) and bulk carbon isotope compositions of the saturated and aromatic hydrocarbon fractions.

Field	Well	Depth (m)	Formation	$\delta^{13}C$ isotope composition (‰)		Rock-Eval pyrolysis data						Bitumen extraction (ppm)	Bulk composition of the extracted bitumen (ppm)			Bulk composition of the extracted bitumen (%)			Saturate/ aromatic ratio
				$\delta^{13}C$ Saturate	$\delta^{13}C$ Aromatic	S (%)	API	Ni (ppm)	V (ppm)	V/ Ni	V/(V + Ni)		Saturate	Aromatic	NSO	Saturate	Aromatic	NSO	
		Late Jurassic Madbi source rock																	
Sunah Oilfield	Sunah-1	2585.0	Madbi									10,800	4664.0	1806.0	4130	44.0	17.04	38.96	2.58
		2585.0										12,000	4680.0	3110.0	4210	39.0	25.92	35.08	1.50
		2586.4		−29.3	−29.7							10,450	6061.0	1579.0	2810	58.0	15.11	26.89	3.84
		2589.0										14,455	6360.2	2834.8	5260	44.0	19.61	36.39	2.24
		2591.3										12,635	5433.0	2957.0	4245	43.0	23.40	33.60	1.84
		2606.5										8235	4282.2	1647.8	2305	52.0	20.01	27.99	2.60
		2610.7		−30.2	−29.7							7075	3537.5	1317.5	2220	50.0	18.62	31.38	2.69
		Middle Jurassic–Lowermost Cretaceous crude oil samples																	
		DST1	Middle Jurassic–Lowermost Cretaceous			0.9	25.0	17.0	19.0	1.12	0.53					54.3	13.90	31.80	3.91
		DST2	reservoir rocks	−29.2	−29.4	1.3	28.0	23.0	25.0	1.09	0.52					61.2	15.10	23.70	4.05
		DST3		−28.3	−28.4	0.6	32.6	5.8	6.0	1.03	0.51					62.8	14.30	22.90	4.39

Table 3
Biomarker ratios of the analyzed seven representative organic-rich shale samples of the Madbi Formation and three oil samples from clastic and carbonate reservoir rocks in the one well location (Sunah-1) in the Sunah Oilfield, Central portion of Say'un-Masilah Basin, illustrating source organic matter, depositional environment conditions and thermal maturity.

Wells	Formation	Depth (m)	Source organic matter and depositional environment conditions														Thermal maturity parameters					
			Pr/ Ph	Pr/ C_{17}	Ph/ C_{18}	CPI	C_{29}/ C_{30}	HCR_{31}/ HC_{30}	DBT/ Phen	Tricyclic terpanes		C_{27}/C_{29} Regular steranes	Diasterane/ Sterane	Regular steranes (%)			C_{32} 22S/ (22S + 22R)	C_{29} 20S/ (20S + 20R)	C_{29} ββ/(ββ + αα)	M_{30}/ C_{30}	MPI	VRC
										C_{26T}/ C_{25T}	C_{23T}/ C_{24T}			C_{27}	C_{28}	C_{29}						
Source rock samples																						
Sunah-1	Madbi	2585.0	1.66	1.00	0.69	0.84																
		2585.0	2.12	0.96	0.60	0.92																
		2586.4	1.80	0.89	0.54	1.02	0.34	0.33	0.42	0.63	2.14	0.73	1.1	33.1	21.7	45.2	0.55	0.41	0.50	0.13	0.54	0.72
		2589.0	2.25	0.97	0.56	0.85																
		2591.3	2.19	1.02	0.62	0.93	0.34	0.31		0.64	1.78	0.70	1.2	32.1	22.2	45.7	0.54	0.43	0.51	0.14		
		2606.5	2.03	1.04	0.60	0.94																
		2610.7	2.25	0.97	0.51	0.94	0.33	0.34	0.12	0.49	1.92	0.81	1.3	36.0	19.5	44.4	0.55	0.40	0.50	0.19	0.57	0.74
Crude oil samples																						
Sunah-1	Middle Jurassic–Lowermost Cretaceous reservoir rocks	DST1	1.57	0.67	0.54	1.01	0.45	0.38		0.57	1.78	0.73	1.3	34.1	14.2	46.7	0.59	0.50	0.56	0.08		
		DST2	1.68	0.67	0.51	0.93	0.45	0.34	1.03	0.69	1.33	0.82	1.2	36.7	18.8	44.5	0.58	0.52	0.59	0.08	0.69	0.81
		DST3	1.60	0.62	0.47	0.97	0.41	0.36	1.05	0.58	1.48	0.87	1.5	37.7	18.8	43.5	0.60	0.55	0.58	0.08	0.70	0.82

Pr = Pristane; Ph = Phytane; CPI = Carbon preference index: $\{2(C_{23} + C_{25} + C_{27} + C_{29})/(C_{22} + 2[C_{24} + C_{26} + C_{28}] + C_{30})\}$; C_{29}/C_{30} = C_{29} norhopane/C_{30} hopane; M_{30}/C_{30} = C_{30} moretane/C_{30} hopane; HCR_{31}/HC_{30} = C_{31} regular homohopane/C_{30} hopane, DBT/Phen = Dibenzothiophene/Phenanthrene, MPI = Methylphenanthrene Index = 1.5 × (2 − MP + 3 − MP)/(Phenanthrene + 1 − MP + 9 − MP), VRC (%) = 0.60 * MPI + 0.40.

Table 4
Basin model input data used to reconstruct the burial and thermal history in the Sunah Oilfield, Central portion of Say'un-Masilah Basin from four well locations as shown in Fig. 4.

Rifting	Formation	Deposition ages		Modelled Wells												Calibration data from Sunah-1 Well				Formation
				High structure (shallower area)						Low structure (deeper area)										
		From	To	Sunah-1 Well			Sunah-2 Well			Pseudo Well A			Pseudo Well B			Vitrinite reflectance (VRo)		Corrected bottom hole temperatures		
				Top	Bottom	Thickness	Top	Bottom	Thickness	Top	Bottom	Thickness	Top	Bottom	Thickness	Depth (m)	Values (% VRo)	Depth (m)	Values (°C)	
																500	0.33			Early
Post-rift	End of early Cretcouse to paleocene sediemnts	58.7	112.0	0.0	1560.0	1560.0	0.0	1486	1486.0	0.0	1540.0	1540.0	0.0	1540.0	1540.0	700	0.39			Cretcouse
	Qishn	112.0	136.4	1560.0	1935.5	375.5	1486.0	1945	459.0	1540.0	1945.0	405.0	1540.0	1918.0	378.0	1000	0.42			
	Saar	136.4	140.2	1935.5	2271.5	336.0	1945.0	2269	324.0	1945.0	2404.0	459.0	1918.0	2269.0	351.0	1200	0.40			
	Nayfa	140.2	150.8	2271.5	2585.0	313.5	2269.0	2539	270.0	2404.0	2836.0	432.0	2269.0	2701.0	432.0	1300	0.39			
Syn-rift																1400	0.36			
	Madbi	150.8	155.7	2585.0	2614.0	29.0	2539.0	2593	54.0	2836.0	2944.0	108.0	2701.0	2917.0	216.0	1620	0.41	1688	66	Qishn
Pre-rift	Shuqra	155.7	161.2	2614.0	2693.0	79.0	2593.0	2674	81.0	2944.0	2996.0	52.0	2917.0	2941.0	24.0	1770	0.44			
	Basement	<170.0	161.2	2693.0	2732.0	39.0	2674.0	2722	48.0	2996.0	3050.0	54.0	2941.0	3030.0	89.0	1920	0.44			
Total depth				2732			2720			3100			3030			1980	0.43			Saar
																2100	0.49			
																2220	0.48			
																2310	0.45	2466	87	Naifa
																2370	0.52			
																2457	0.58			
																2588	0.63			Madbi
																2591	0.69			
																2605	0.67			
																2610	0.73			
																2680	0.71	2666	102	Shuqra
																		2683	102	
																		2689	103	
																		2694	104	

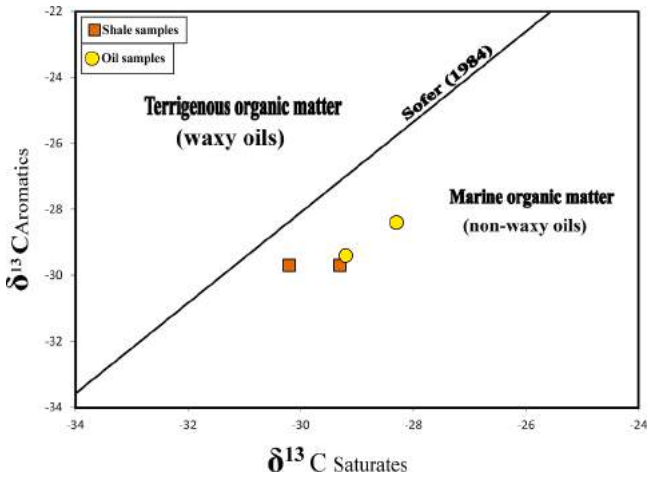

Fig. 4. "Sofer plot" of δ^{13}Caroversus δ^{13}Csat for the oil samples and extracted Madbi shale samples from Sunah Well in the Sunah Oilfield. The dotted line represents the best fit separation for waxy and non-waxy oils and is described by the equation δ^{13}Caro = 1.14 δ13Csat + 5.46 (Sofer, 1984).

selected samples were prepared as polished blocks by mounting fine grades of crushed rock samples (≤1 mm in size) inside a slow setting polyester of Serrifix resin mixed with resin hardener, later hardening. The mean vitrinite reflectance (%VRo) values were measured using oil immersion and observed under a Zeiss microscope and Leitz Orthoplan/MPV photometric system under a white plane-polarized reflected light.

3.3. PetroMod 1D modeling dataset

In this study, the basin modeling, involving burial and thermal maturity over geological time, of the Sunah oilfield was conducted using the PetroMod 1D modeling software. The procedure of burial and the thermal models were constructed through several geological factors, including tectonic, width, and lithologic properties of rocks, as well as the maturity of sedimentary successions in the basin. In this regard, the burial models were constructed using geological data inputs such as sedimentary rock types and thickness extracted from unpublished compilation reports and schematic geological cross-sections from SW to NE in the Sunah oilfield (Fig. 4 and Table 3). The timing of deposition and erosion events was provided by the Lexique Stratigraphic International of Yemen, as described by Beydoun et al. (1998) and As-Saruri et al. (2010).

Other input data like the boundary conditions, including thermal gradient and heat flow (HF, mW/m^2), are used to model the thermal background of the basin and then source rock maturation (Lachenbruch 1970; Welte et al., 2012; Allen and Allen, 1990). The HF is assumed from the mantle as a result of tectonic evolution and heat of radioactivity that formed from crustal (Allen and Allen, 1990; 2005; Hantschel and Kauerauf, 2009).

The paleo-heat flow values were commonly estimated from thermal maturity calibration data, such as measured vitrinite reflectance (%VRo) and Rock-Eval T_{max} (e.g., Makeen et al., 2016; Shalaby et al., 2011; He and Middleton, 2002). In this regard, several models of thermal maturity were used using Sweeney and Burnham's (1990; EASY% Ro) thermal modeling approach.

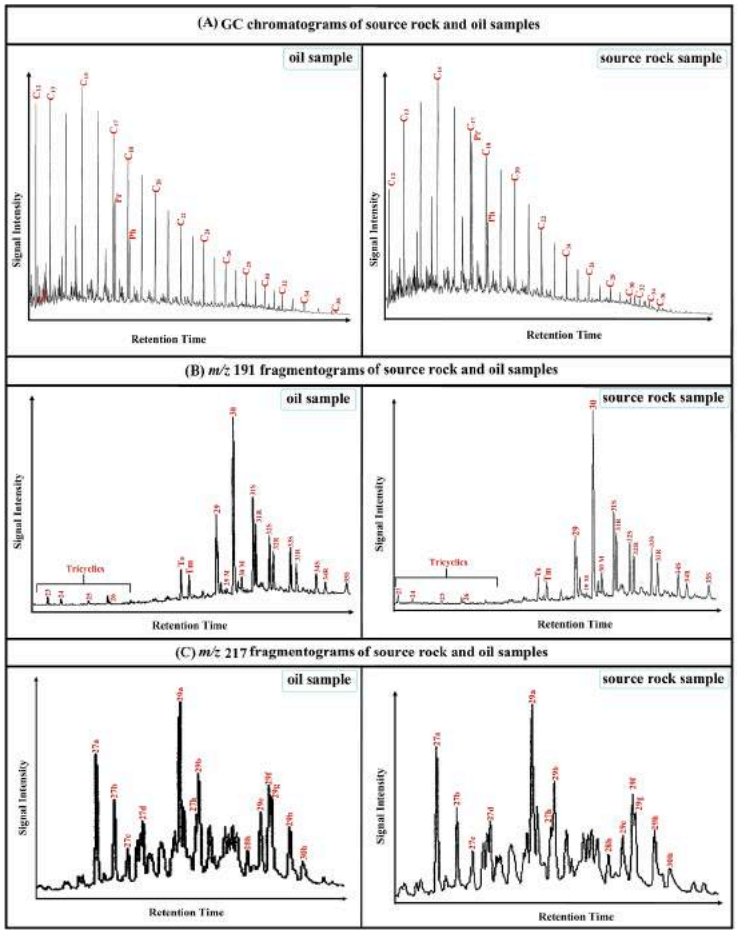

Peak m/z 191	Compound	abbreviation
Ts	18α(H),22,29,30-trisnorneohopane	Ts
Tm	17α(H),22,29,30-trisnorhopane	Tm
29	17α,21β(H)-nor-hopane	C_{29} hop
30	17α,21β(H)-hopane	Hopane
30M	17 β,21α (H)-Moretane	C_{30}Mor
31S	17α,21β(H)-homohopane (22S)	C_{31}(22S)
31R	17α,21β(H)-homohopane (22R)	C_{31}(22R)
32S	17α,21β(H)-homohopane (22S)	C_{32}(22S)
32R	17α,21β(H)-homohopane (22R)	C_{32}(22R)
33S	17α,21β(H)-homohopane (22S)	C_{33}(22S)
33R	17α,21β(H)-homohopane (22R)	C_{33}(22R)
34S	17α,21β(H)-homohopane (22S)	C_{34}(22S)
34R	17α,21β(H)-homohopane (22R)	C_{34}(22R)
35S	17α,21β(H)-homohopane (22S)	C_{35}(22S)
35R	17α,21β(H)-homohopane (22R)	C_{35}(22R)

Peak m/z 217	Compound	abbreviation
a	13β,17α(H)-diasteranes 20S	Diasteranes
b	13β,17α(H)-diasteranes 20R	Diasteranes
c	13α,17β(H)-diasteranes 20S	Diasteranes
d	13α,17β(H)-diasteranes 20R	Diasteranes
e	5α,14α(H), 17α(H)-steranes 20S	ααα20S
f	5α,14β(H), 17β(H)-steranes 20R	αββ20R
g	5α,14β(H), 17β(H)-steranes 20S	αββ20S
h	5α,14α(H), 17α(H)-steranes 20R	ααα20R

Fig. 5. Gas chromatograms, *m/z* 191 and *m/z* 217 mass fragmentograms in the saturated hydrocarbon for representative analyzed oil and extracted Madbi shale rock samples from Sunah Well in the Sunah Oilfield.

In addition to paleo-heat flow estimation, the present-day heat flow values were also calculated within the PetroMod 1D program by calibrating the thermal conductivity of the rock units and subsurface geothermal gradients. In this study, the geothermal gradients are determined using the bottom hole temperature (BHT) in the studied well, as shown in Table 4. However, the default thermal conductivity values of the rock units in the PetroMod basin modeling software were used in this study.

Furthermore, the petroleum generation and expulsion over geological time were simulated and modeled through different source rock organic facies, including geochemical data of TOC content and HI. During the petroleum generation modeling, the Madbi source rock was modeled as a Type II source rock, and the oil generation from Type II kerogen was modeled at each burial history using the Tissot et al. (1987) T2 (Type II) kinetic parameters. The primary and secondary reaction kinetic aspects of Type II oil-source rock, however, were integrated with the burial history and thermal maturity of the rock to record the time of oil generation and expulsion in this Type II kinetic model.

4. Results

4.1. TOC/RE pyrolysis and bitumen extraction

TOC/RE pyrolysis data are made available for all the Madbi shale samples in the studied Sunah-1 well, as summarized in Table 1.

The TOC content is often used to evaluate the organic matter content and its ability to produce petroleum during maturity (Jarvie, 1991; Peters and Cassa, 1994). The analyzed Madbi shale samples possess a high level of organic matter, as indicated by a TOC content of up to 12 wt % (Table 1). According to Bissada (1982) and Katz and Lin (2014), most of the favorable source rocks had a TOC level of more than 1%.

Table 1 also shows the geochemical parameters of twenty samples of the studied Madbi shales that were subjected to programmed pyrolysis analysis. These pyrolysis parameters, coupled with TOC content, were utilized to evaluate the amount and quality of organic matter in the Al Renk shales along with their thermal maturity (Espitalie et al., 1977; Espitalie et al., 1985).

In this study, the petroleum yields of S_1 and S_2 in the analyzed shale samples show high values of 3.2–8.1 mg and 12.65–70.43 mg HC/g rock, respectively (Table 1). The S_3 peak, which reflects the quantity of CO_2 generated by the pyrolysis of organic matter, was produced during programmed pyrolysis and found to be 0.34–0.99 mg CO_2/g rock (Table 1). The S_2 and S_3 yields are compatible with TOC content and used to calculate HI and OI values, according to Peters and Cassa (1994). The bulk pyrolysis results like HI and OI were outlined for all 20 analyzed Madbi shale samples (Table 1), then used to identify the types of kerogen (e.g., Peters and Cassa, 1994; Mukhopadhyay et al., 1995). In this study, the HI and OI values were found to be 431–613 mg HC/g TOC and 4–20 mg CO_2/g TOC, respectively (Table 1).

The majority of the samples (n = 16) have high HI values of over 500 mg HC/g TOC (501–613 mg HC/g TOC), while four samples have relatively lower HI values (431–495 mg HC/g TOC). In terms of OI values, the majority of the analyzed samples (n = 11) have high OI values of 10–20 CO_2/g TOC, whilst the other nine samples have relatively low OI values of less than 10, varying from 4 to 9 CO_2/g TOC (Table 1).

During the pyrolysis investigation, the maximum temperature (T_{max}) of the S_2 peak and PI values of the shale samples were also obtained (Table 1). T_{max} values with S_2 yielding higher than 1 mg/g rock provide the most reliable results (Jarvie et al., 2001; Katz and Lin, 2021). Hence, most of the analyzed samples have reliable T_{max} results varying from 432 to 444 °C (Table 1). Five analyzed samples have T_{max} values less than 440 °C (432–439 °C), whilst the other samples have relatively higher T_{max} values of 440–444 °C (Table 1).

Furthermore, the amounts of free bitumen extracted from representative analyzed samples ranged between 7075 and 14455 ppm (Table 2), consistent with a high TOC content, which further suggests that significant petroleum can be generated from the analyzed shale samples (Peters and Cassa, 1994). Furthermore, the bulk compositions of the extracted bitumen, including saturated, aromatic hydrocarbons, and NSO polar, are measured and presented in Table 2. The distributions of the bulk composition show that the extracted bitumen from the rock samples is dominated by saturated hydrocarbon, with a volume of 39–58%. The notable amounts of NSO polar are also present in 26.89–38.96% of the volume, followed by relatively low amounts of aromatic hydrocarbons (15.11–25.92%). However, the significant amounts of NSO contents are attributed to the relatively low maturity level of the analyzed Madbi shale samples (e.g., Peters et al., 2005).

4.2. Physical and geochemical fingerprints of crude oils

The API gravity value and total sulfur content in the examined oils are measured and found to be 25.0–32.6 and 0.6–1.3 wt%, respectively (Table 2). The physical property of the API gravity was combined with the total sulfur and used to assess the difference between kerogen Type II and Type II-S (Orr, 2001). The inorganic elements of Ni and V metals within the examined oil samples were evaluated when in their lowest amounts of 5.8–23.0 ppm and 6.0–25.0 ppm, respectively (Table 2). These measured values of V and Ni trace elements in the oils were also used to calculate several ratios such as V/N and V/(V + Ni), which were widely used to highlight the depositional conditions of their probable source rocks (Wenger et al., 2002; Galarraga et al., 2008).

In addition, the examined oil samples were segmented into aromatics saturates and polar (NSO) components and their comparative fragments were calculated and presented in Table 2. The examined oil samples have a higher saturated fraction than other fractions, reaching more than 50%, followed by polar compounds with a volume of 22.90–31.80% (Table 2). Such enrichment in saturated HC commonly exists in naturally generated crude oil (Lewan et al., 2006). The saturated hydrocarbon dominance is attributed to the maturation of the petroleum source rocks and indicates source rocks with high thermal maturity for most of the crude oil samples. The aromatic hydrocarbon is the lowest fraction in all oil samples, with a volume of 13.90–15.10%, resulting in high saturate/aromatic HC ratio between 3.91 and 4.39 (Table 2).

4.3. Bulk carbon stable isotope ($\delta^{13}C$) compositions

In this study, a bulk stable $\delta^{13}C$ analysis was conducted on the aliphatic and aromatic hydrocarbon fractions of both Madbi shale samples and crude oils. The results indicate that the bulk $\delta^{13}C$ values of the saturated and aromatic portions are −28.3‰ to −30.2‰ and −28.7‰ to −29.7‰, respectively (Table 2). Such saturated and aromatic $\delta^{13}C$ values are widely used to classify crude oils and to demonstrate the nature of organic matter inputs of their probable source rocks, thereby contributing toward investigating the genetic composition of the oils (Sofer, 1984). High and moderate $\delta^{13}C$ values are thought to originate from aquatic algae and microorganisms, whereas low $\delta^{13}C$ values indicate a predominantly terrigenous origin (Sofer, 1984). Accordingly, the examined oil samples are primarily non-waxy oils and appear to generally be derived from source rock riches in marine organic matter, as indicated from a Sofer (1984) plot (Fig. 4). The relationship among the saturated and aromatic hydrocarbon fractions of their stable $\delta^{13}C$ composition reveals that the bulk $\delta^{13}C$ values of the examined oils are consistent with the Madbi shale rocks (Fig. 4). This finding suggests that there is a genetic link between the examined oils with those of the analyzed shale samples within the Late Jurassic Madbi Formation.

4.4. Biomarker fingerprint of organic matter

4.4.1. Normal-alkanes and acyclic isoprenoids

Organic biomarker fingerprints in the saturated fraction of extracted

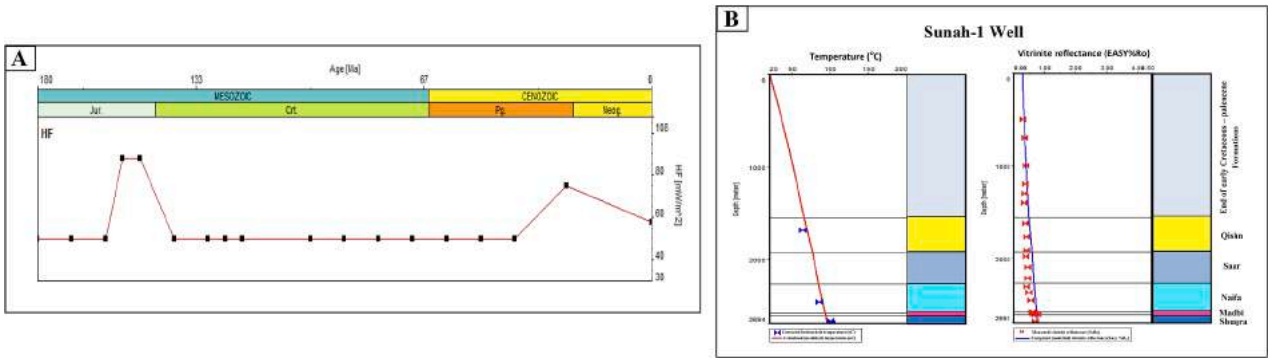

Fig. 6. Basin model for the studied well (Sunah-1), showing heat flow evolution in the Say'un-Masilah Basin. This estimated heat flow range is achieved from optimized fit of measured calibration data [i.e. bottom-hole temperatures and measured vitrinite reflectance (%VR)] and calculated models of EASY %Ro maturity and geothermal models in the studied Sunah-1 Well.

rocks and examined oils are commonly detected from the chromatograms of GC (Fig. 5a). Both the extracted rocks and oils have significantly low *n*-alkane numbers and acyclic isoprenoids in the chromatogram (Fig. 5a), indicating that the analyzed oil samples are not biodegraded samples. The *n*-alkanes are characterized by a distribution of unimodal of C_{12} and C_{36}, ranging from short- and medium-chain n-alkanes between C_{13} and C_{24} (Fig. 5a). This distribution of normal alkanes results in low carbon preference index (CPI) values of 0.84–1.02 (Table 3).

The chromatograms also show the presence of significant amounts of pristane (Pr) and phytane (Ph) acyclic isoprenoids in all examined extracted rocks and oils (Fig. 5a). These geochemical biomarkers of isoprenoid hydrocarbons and their ratios are commonly used to highlight organic matter inputs and their depositional environment conditions (e.g., Chandra et al., 1994; Didyk et al., 1978). The Pr acyclic isoprenoid was more than Ph in all the analyzed extracted rock and oil samples (Fig. 5a), resulting in Pr/Ph ratio values of 1.57–2.25 (Table 3). However, the oil samples have relatively lower Pr/Ph (<1.70) values than the extracted rocks (Table 3). In addition, the acyclic isoprenoids are compatible with the *n*-alkanes of C_{17} and C_{18}, providing values of 0.62–1.04 and 0.47–0.69 for Pr/*n*-C_{17} and Ph/*n*-C_{18} ratios, respectively (Table 3).

4.4.2. Hopanoid and steroids

The biomarkers of hopanoid and steroid compounds are also present in the saturated hydrocarbon fraction of the examined extracted rocks and oils, commonly detected from *m/z* 191 and 217 mass fragmentograms (Fig. 5b and 5c).

Mass fragmentograms of *m/z* 191 ion in both extracted rock and examined oil samples display a large amount of hopanes compared to tricyclic terpanes (Fig. 5b), including 17α (H)-trisnorneohopane (Tm), 18α (H)-trisnorneohopane (Ts), homohopanes of C_{31}–C_{35}, C_{30} hopane, and C_{29} norhopane. The higher abundance of C_{30} hopanes than C_{29} norhopanes in the analyzed samples (Fig. 5b) resulted in low C_{29}/C_{30} hopane values of less than 1 and suggested typical clay-rich facies, as reported by Gürgey (1999).

The homohopanes of C_{31}–C_{35} from both extracted rocks and examined oil samples are dominated by C_{31} and decline to C_{35} homohopanes (Fig. 5b). The ratio of C_{31} R/C_{30} hopane was calculated based on the compatibility between the distribution of the homohopane C_{31}22R series and the C_{30} hopane (Fig. 5b), giving high values of 0.31–0.38 (Table 3), suggesting a marine depositional environment (e.g., Peters et al., 2005). Additionally, low quantities of tricyclic terpanes are also detected in mass fragmentograms of *m/z* 191 ion (Fig. 5b), and their several ratios such as C_{23} tricyclic/C_{24} tricyclic (C_{23}/C_{24}) and C_{25} tricyclic/C_{26} tricyclic (C_{26}/C_{25}Tr) were also calculated (Table 3).

Other important biomarker compounds recognized in the *m/z* 217 are steroids, showing that diasteranes dominate over steranes (Fig. 5c), giving a high diasterane/sterane ratio between 1.1 and 1.3 in the analyzed rocks and oils (Table 3). A higher diasteranes over steranes ratio further suggests the lithology of clay-rich sediments (e.g., Hakimi et al., 2011; Peters et al., 2005). The analyzed samples also show the comparative abundance of standard regular steranes of C_{27} to C_{29} in the *m/z* 217 mass fragmentograms, which are characterized by high amounts of C_{29} and C_{27} regular steranes relative to C_{28} regular sterane (Fig. 5c). The relative proportion of C_{29}, C_{27}, and C_{28} regular steranes is estimated and found to be 43.5–46.7%, 32.1–37.7%, and 14.2–22.2%, respectively (Table 3). Other sterane ratios such as ββ/(ββ + αα) and 20S/(20S + 20R) of C_{29} sterane as well as C_{27}/C_{29} regular sterane were also calculated (Table 3).

4.4.3. Certain aromatic biomarkers

In the current study, the chromatograms of *m/z* 184, *m/z* 178, and *m/z* 192 ions in the aromatic fractions of the investigated four samples (two extracted rock samples and two oil samples) were examined to obtain certain aromatic biomarkers of phenanthrene (P), methylphenanthrene, and dibenzothiophene (DBT) and further calculate their DBT/P, MPI, and calculated reflectance (VRc) parameters (Table 3). As such, these aromatic parameters and ratios were applied to evaluate the thermal maturity of the organic matter (e.g., Radke et al., 1986; Chakhmakhchev and Suzuki, 1995) and outline the lithologies of source facies and their depositional environment (Hughes et al., 1995). The ratio of dibenzothiophene/phenanthrene (DBT/P) was calculated on the basis of isomer distribution of aromatic compounds in *m/z* 184 and 178 ions and ranged from 0.12 to 0.42 and 1.03 to 1.05 for exacted rocks and oil samples, respectively (Table 3). Such DBT/P can provide information on the depositional environment of source rocks and their lithology facies (e.g., Hughes et al., 1995). Other aromatic maturity indicators calculated for the analyzed samples include MPI and equivalent VRc (Table 3). The exacted rocks and oil samples have values of MPI ranging from 0.54 to 0.57 and 0.69 to 0.70, respectively. From the MPI parameter, the VRc values of the exacted rocks and oil samples were calculated as 0.72–0.74% and 0.81–0.82%, respectively (Table 3).

4.5. Thermal maturity geo-history modeling

In this study, the burial and thermal geo-history models were reconstructed using four wells (Sunah-1, Sunah-2, Pseudo-A, and Pseudo-B) obtained from seismic interpretations in the Sunah oilfield (Fig. 3). The geothermal history was generally established using a paleo HF, generally assumed based on the subsidence activities, and highlighted the main tectonic events (Lachenbruch, 1970; Allen and Allen, 1990).

The HF values in the Sunah oilfield were estimated by the basin modeling task using the availability of calibration maturity data such as vitrinite reflectance (%VRo) and corrected bottom hole temperature

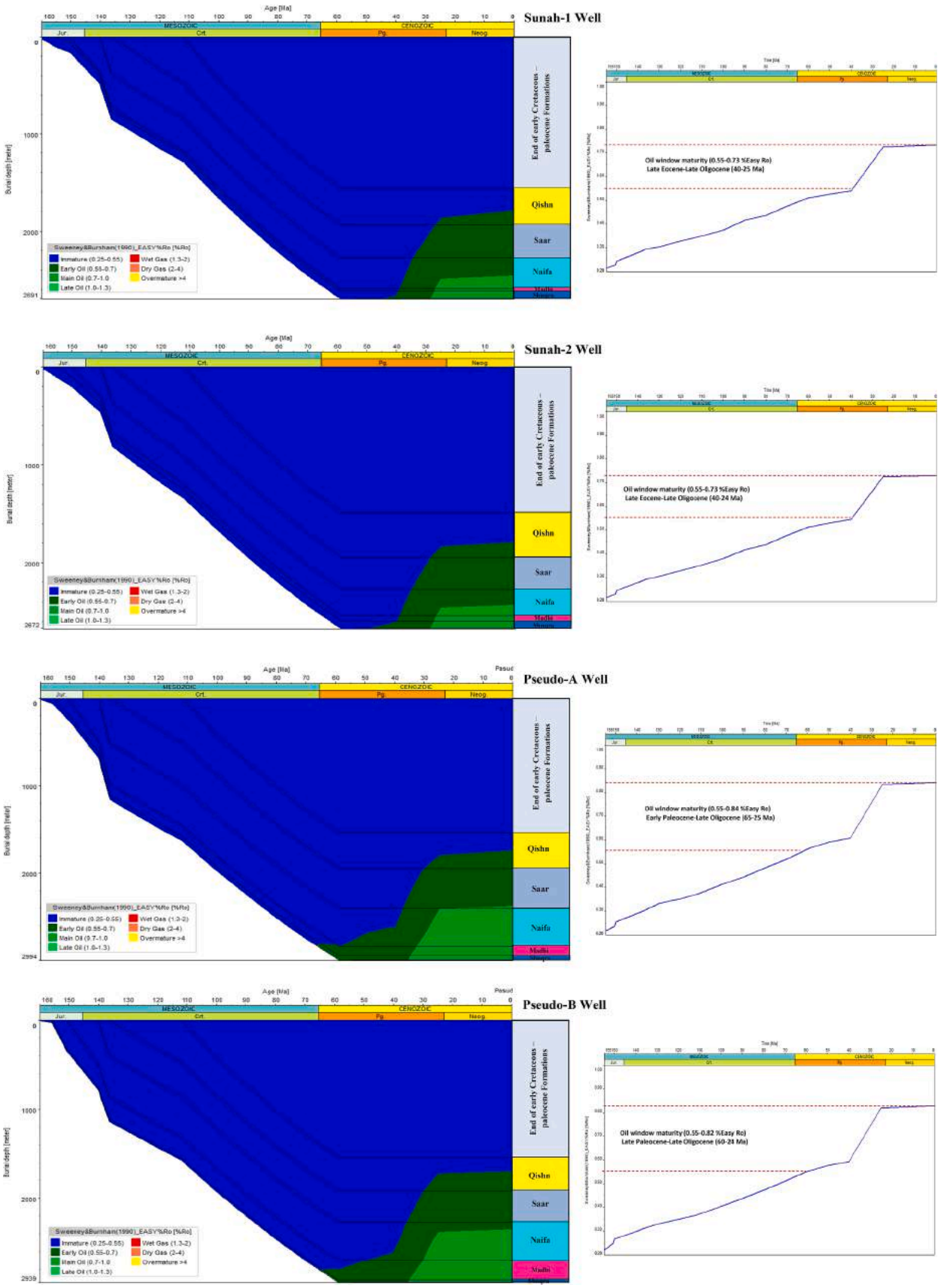

Fig. 7. 1D basin models of the burial overlap with thermal maturity (colored areas) cross all rock units (left) and blue lines are shown exclusively for computed vitrinite reflectance of the base Madbi source rock set for four well locations (Sunah-1, Sunah-2, Pseudo-A and Pseudo-B) in the structural highs and deeper area of the Sunah Oilfield as shown in Fig. 3. (For interpretation of the references to color in this figure legend, the reader is referred to the web version of this article.)

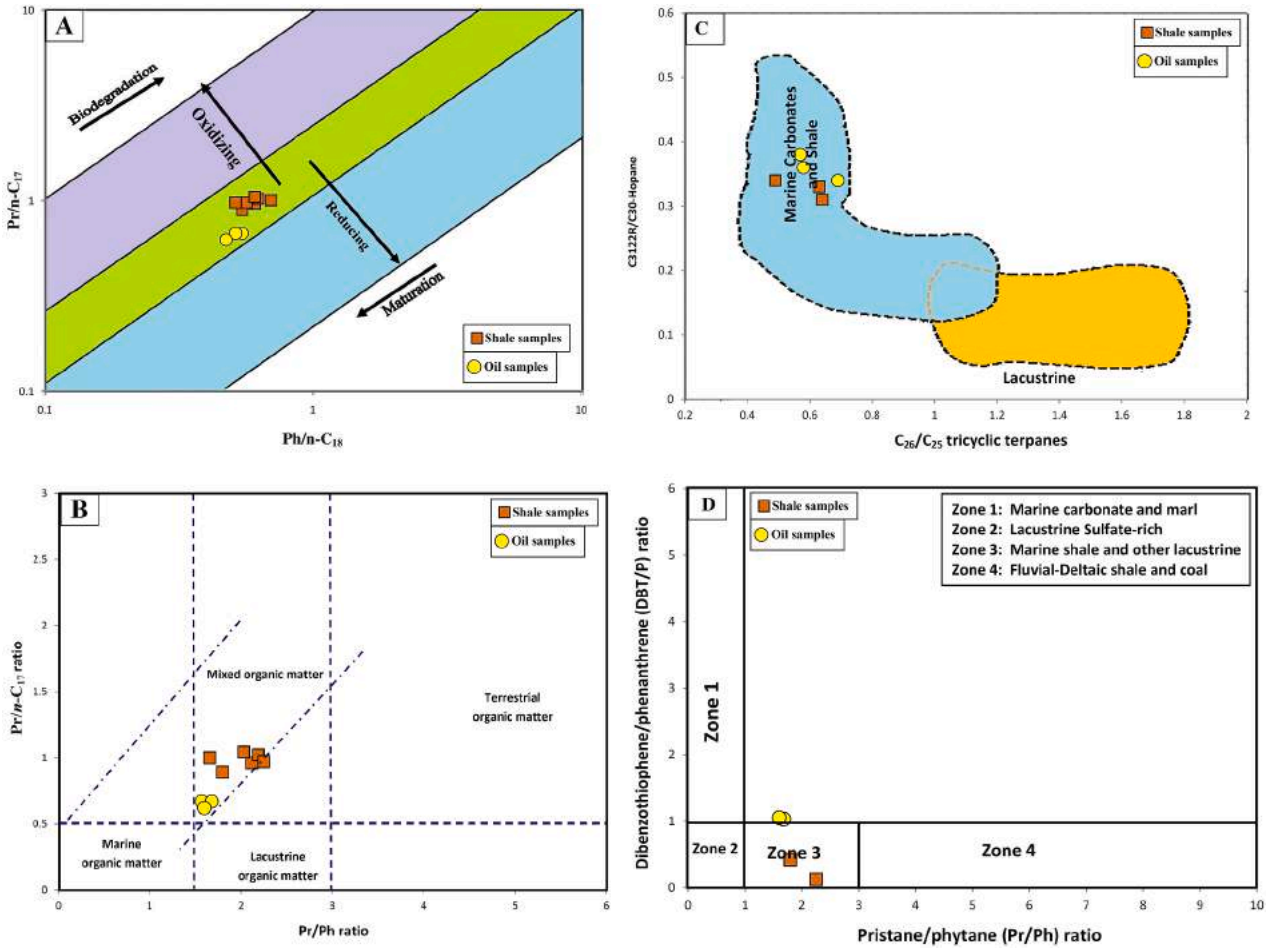

Fig. 8. Geochemical biomarker results of the oil samples and extracted Madbi shale rocks from Sunah Well in the Sunah Oilfield: (a) pristane/*n*-C_{17} versus phytane/*n*-C_{18} (from Shanmugam, 1985), and (b) pristane/phytane versus pristane/*n*-C_{17}, (c) $C_{31}R/C_{30}$ hopane versus C_{26}/C_{22} tricyclic (from Peters et al., 2005), and (d) DBT/Phen versus Pr/Ph (from Hughes et al., 1995), indication generally genetic link between the oil and Madbi shale samples.

(BHT) (Table 4). In this respect, the values of HF being studies were estimated to be 50–90 mW/m^2 (Fig. 6a), as achieved from matching between the models and measured data of %VRo and BHT in the studied Sunah-1 well (Fig. 6b). The adopted HF model also shows high values between 78 and 90 mW/m^2 of paleo HF during the Late Jurassic and late Oligocene, respectively (Fig. 6a). These high values are most likely attributable to the rifting systems in the basin during the Late Jurassic–Early Cretaceous and Oligocene–Miocene (e.g., Redfern and Jones, 1995; As-Saruri et al., 2010). This HF model was further incorporated with burial temperatures in the studied wells (Sunah-1, Sunah-2, Pseudo-A, and Pseudo-B) along the Sunah oilfield and applied as the major factors that controlled the thermal maturity stage. Thereby the model was used to simulate the conversion of organic matter in the Madbi source rock into oil over geological time.

Fig. 7 presents the models of burial and thermal geo-history in the studied wells, showing that the base of the Madbi Formation (source rock) had a burial depth within the range of 2539 m and 2944 m (Table 4) and reached the mature stage of the oil window during the late Oligocene (at the age 25–24 Ma) as demonstrated from modeled VR values between 0.70 and 0.83 EASY% Ro (Fig. 7).

The thermal history models also outline that the early oil-generation window of 0.55 Easy% Ro was entered in the Madbi source rock at the geological ages of the early Paleocene and late Eocene (Fig. 7). From the late Oligocene to date, the peak oil window of VR values between 0.73 and 0.84 %Ro took place in the Madbi source rock (Fig. 7). However, the thermal history models also show that the Madbi source rock in the Pseudo-A and -B wells is more mature compared to the Sunah-1 and -2 wells (Fig. 7). This difference in thermal maturities is probably attributed to the variations in burial depth of the Madbi Formation across the studied wells. Thus, the Madbi Formation in the known deeper areas (i.e., Pseudo-A and -B wells) is defined as an effective source rock and, consequently, yields/generates commercial amounts of oil.

5. Discussion

5.1. Organic matter input and environmental conditions for source rock

Organic matter input source in the Late Jurassic Madbi source rock and their likely origin were determined by applying multi geochemical proxies, including organic molecular biomarkers and bulk $\delta^{13}C$ compositions, together with microscopic results. The organic molecular biomarkers, such as normal alkanes, isoprenoids, terpanes, and steranes, and their ratios and parameters were used (Table 3). As shown from hydrocarbon distributions, the normal alkanes of the lipid biomarker in the saturated HCs showed a unimodal of high abundance of C_{12}–C_{20} to middle C_{21}–C_{25} carbon numbers (Fig. 5a), suggesting that these Madbi shale sediments contain high numbers of marine organisms with a volume of terrigenous OM input (Gelpi et al., 1970; Cranwell, 1977; Mansour et al., 2020; Gharib et al., 2021; Hadad et al., 2021). The higher contributions from the marine organic matter into these shale sediments confirm a Sofer (1984) plot of the $\delta^{13}C$ values of their saturated and aromatic hydrocarbon fractions (Fig. 4). However, the interference of the organic matter inputs is also in line with the CPI values (Peters et al., 2005). Data shows that the CPI values of most samples are less than 1,

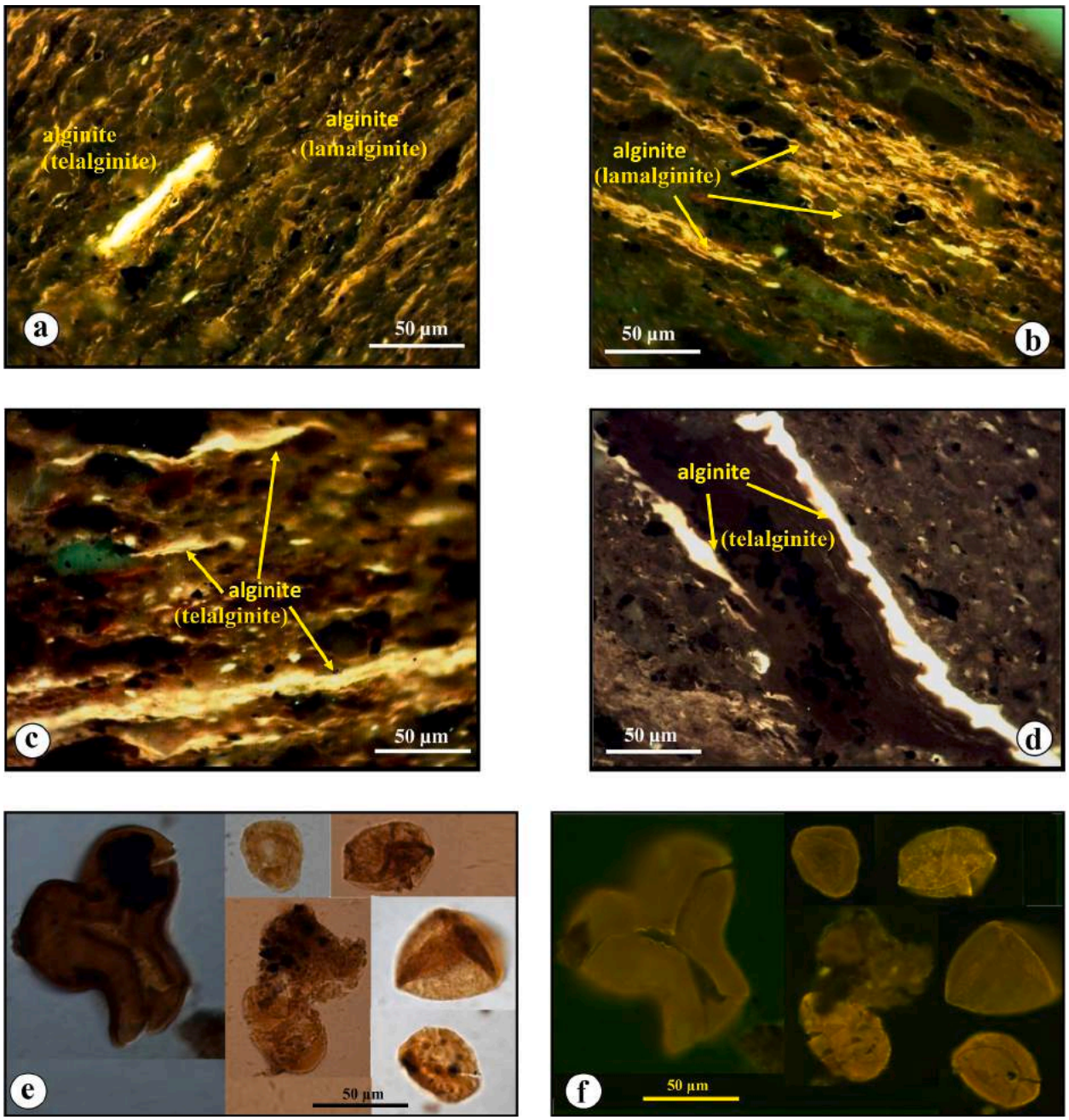

Fig. 9. Photomicrographs of organic matter assemblage from the Madbi shale source rock in the Kharir Oilfield; under reflected and transmitted lights, field width = 0.2 mm: (a-d) alginite organic matter with varied fluorescence color from yellow to bright yellow fluorescence under UV reflected light, showing telalginite and lamalginite forms, (e) palynomorph assemblage (i.e. spores and pollens) under white transmitted light and (f) dark yellow to bright yellow fluorescence colours of the palynomorph assemblage. (For interpretation of the references to color in this figure legend, the reader is referred to the web version of this article.)

whereas 10% are higher than 1 (Table 1), therefore further supporting the interpretation of a mixture of organic matter input with large amounts of marine organic matter input (Peters et al., 2005). Further, the combination between the isoprenoids ratios such as Pr/Ph, Pr/C_{17}, and Ph/C_{18} is also used to interpret the contribution from the organic matter and their depositional circumstances (Tserolas et al., 2019).

The lower Pr concentrations compared with Ph reveal the higher contributions of aquatic organic matter and act as a critical sign of the redox conditions during the sedimentation and diagenesis (Large and Gize, 1996; Rowland et al., 1993). The Pr/Ph ratio of less than 1 indicates an anoxic environment associated with a laminated water column, while Pr/Ph of greater than 3 is related to high contributions from terrestrial organic matter during oxic environmental circumstances, as reported previously (Didyk et al., 1978; Ten Haven et al., 1987; Chandra et al., 1994).

The majority of the investigated Madbi shale samples showed relatively higher Pr/Ph, ranging from 1.66 to 2.25 (as shown in Table 3), indicating that these shale specimens carry a mixture of organic matter and accumulated during relatively reducing (suboxic) environmental conditions during deposition. This finding is demonstrated by the relationship between pristane/*n*-C_{17} and phytane/*n*-C_{18} ratios (Fig. 8a). The reducing conditions during deposition consequently enhanced the preservation, which subsequently caused the enrichment of organic matter in the Madbi shale sediments, as indicated by the high TOC values of up to 12 wt% (Table 1). This finding is consistent with the presence of algae as *telalginite* and *lamalginite* (Fig. 9a–d), which are

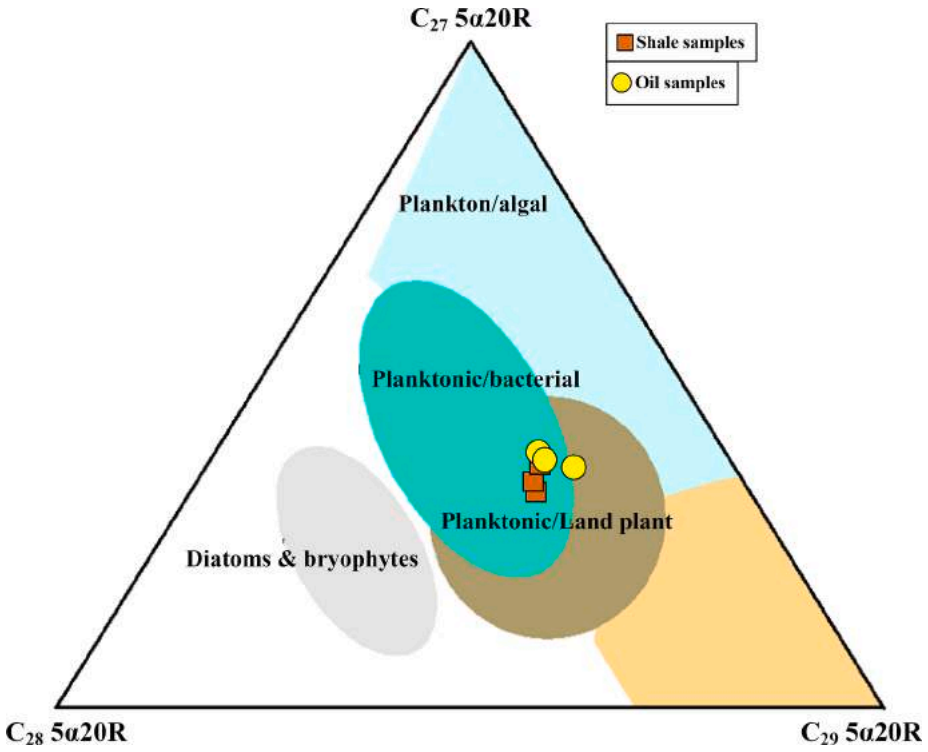

Fig. 10. Ternary diagram of regular steranes (C_{27}-C_{29}) in the oil samples and extracted Madbi shale rocks from Sunah Well in the Sunah Oilfield, indicating the relationship between sterane compositions, concerning organic matter input (modified after Huang and Meinschein, 1979).

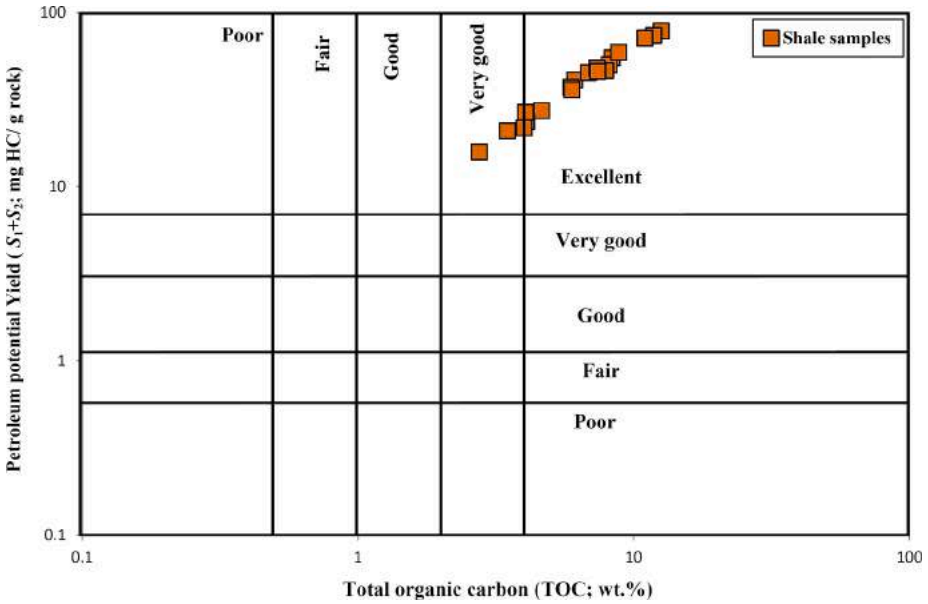

Fig. 11. The plot of total organic carbon (TOC) content vs. petroleum potential yield ($S_1 + S_2$), showing the analyzed Madbi shale samples are very good to excellent source rocks for petroleum generation potential (Adapted from Shalaby et al., 2012).

typical of marine algae accumulated under reducing conditions (Tyson, 1995; Taylor et al., 1998; Bornemann et al., 2003). The occurrence of reducing conditions consequently enhanced the growth of algae and marine microorganisms owing to the presence of abundant nutrients (Tyson, 1995; Taylor et al., 1998; Hakimi et al., 2016).

In addition, the combination between the isoprenoid ratios of Pr/Ph and Pr/*n*-C_{17} has also been used to distinguish between the contributions from marine and non-marine organic matter (as reported by Hughes et al., 1995; Hakimi et al., 2012; Sarki Yandoka et al., 2015). Accordingly, the investigated Madbi shales received a mixture of marine and terrestrial organic matter as implied by the relatively high Pr/Ph and Pr/*n*C_{17} (Fig. 8b). Furthermore, the presence of the low amounts of plant organic matter also suggests that the relatively high proportions of Ts than Tm in the aliphatic hydrocarbon fraction of the analyzed Madbi shale samples (Fig. 12) is indicative of organic matter derived from land plants (e.g., Sarki Yandoka et al., 2015).

This finding is compatible with the distribution of the tricyclic terpane biomarkers and their ratios, which are typical of aquatic-derived

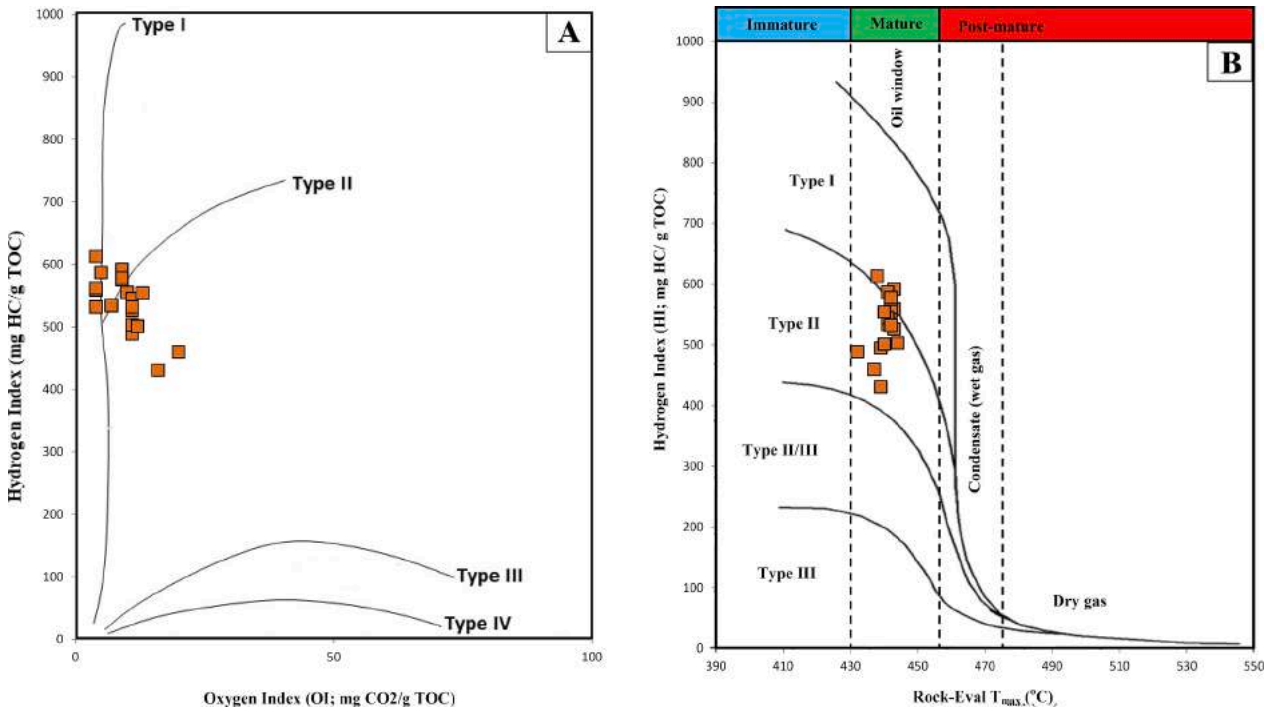

Fig. 12. Geochemical correlations between hydrogen index (HI), oxygen index (OI) (adapted from Espitalie et al., 1977), and T_{max} (adapted from Espitalie et al., 1985). The analyzed organic-rich shales within the Madbi Formation are dominated by Type II kerogen.

organic matter (Zumberge, 1987; Hanson et al., 2000). In this respect, the high values of the C_{23}/C_{24} tricyclic terpane ratio are compatible with the low C_{26}/C_{25} tricyclic terpane ratio of less than 1 (Table 3) and suggest high amounts of marine organisms of algae and bacteria accumulated at the deposition time of the analyzed shale sediments. Furthermore, the combination between the ratios of DBT/Phen, Pr/Ph, $C_{31}R/C_{30}H$, and C_{26}/C_{25} tricyclic terpane is a good indicator for marine origin (Fig. 8c and 8d).

These recognized organic facies are further underscored by the homologous series of C_{27}–C_{29} regular sterane in the *m/z* 217 ion fragmentogram (Fig. 5c). Accordingly, the distribution of C_{27}–C_{29} regular steranes reflects an accumulation of mixed organic matter, with high contributions of planktonic-bacterial organic matter and minute contributions of land plants to the source rock, as noticed from the concentration plot of C_{27}–C_{29} steranes on a ternary diagram (Fig. 10). However, the dominance of the C_{27} and C_{29} regular steranes is good indicators for the presence of red and green algae in the analyzed samples (e.g., Schwark and Empt, 2006). The high source of planktonic organic matter, algal with a minute terrestrial plant contribution, is compatible with significant fluorescent characteristic assemblages (Fig. 9a–d) with other terrestrial materials (i.e., spores and pollens) observed under light microscopy (Fig. 9e and 9f). The dominant presence of phytoplankton algae in the Madbi shale sediments suggests warm water and anoxic conditions during the Late Jurassic (Tyson, 1995) that enhanced the abundance of primary nutrients in seawater and would likely have caused the high bioproductivity of phytoplankton blooms. The presence of warm water and reducing conditions during the Late Jurassic enhanced both the preservation and bioproductivity of organisms, thereby causing the enrichment of organic matter in the Madbi shale sediments, as indicated by the high TOC values of up to 12 wt% (Table 1).

5.2. Source rock characteristics and hydrocarbon generation potential

The section above discussed the organic matter (kerogen) characteristics and highlighted the implication for source rock attributes of the shale intervals within the Madbi Formation based on both organic geochemical and petrological results. These results also highlight the petroleum generation potential that can generally be investigated from the organic matter input into the Madbi shales and their thermal maturation via burial temperatures.

The presence of adequate volumes of organic matter is a critical factor to control the petroleum generation once thermal maturity is attained (e.g., Peters and Cassa, 1994; Ardakania et al., 2017; Makeen et al., 2019). The organic richness within the sediments and their generative potential are gauged through TOC, and hence, it is one of the most critical geochemical parameters (Bissada, 1982; Jarvie, 1991; Peters and Cassa, 1994; Katz and Lin 2014; Qadri et al., 2016).

The present study shows TOC results (TOC > 2; maximum TOC value = 12 wt%) from the investigated Madbi shale (Table 1). These values are enough to support the Madbi shale sediments as a host for a higher concentration of organic matter and would be considered a favorable source rock (Bissada, 1982; Katz and Lin, 2014), which is consistent with the presence of the enrichment of organic matter in these shale sediments. The enrichment of organic matter in most of the analyzed Madbi shale samples suggests the preservation of organic matter due to low oxygen conditions during the deposition time, as demonstrated from the biomarker results (see Section 5.1).

However, the generative generation potential of the Madbi shale samples was demonstrated by the correlation between the TOC results and the petroleum potential (S_2) yields. This relation implies an excellent source rocks category and a better indication of high contributions of petroleum generation potential from Madbi shale samples (Fig. 11). The contribution of organic matter and type of kerogen within the studied Madbi organic-rich shale samples and their characteristics is a second critical step in predicting the petroleum type (oil or/and gas) generated during thermal maturation.

The RE parameters such as HI and OI were employed to conduct the qualitative kerogen classification diagrams (Espitalie et al., 1985; Peters and Cassa, 1994). These parameters suggest that the characteristics of the organic facies are similar and that the Type II kerogen is the main organic matter in the analyzed Madbi shale samples, as reflected from a

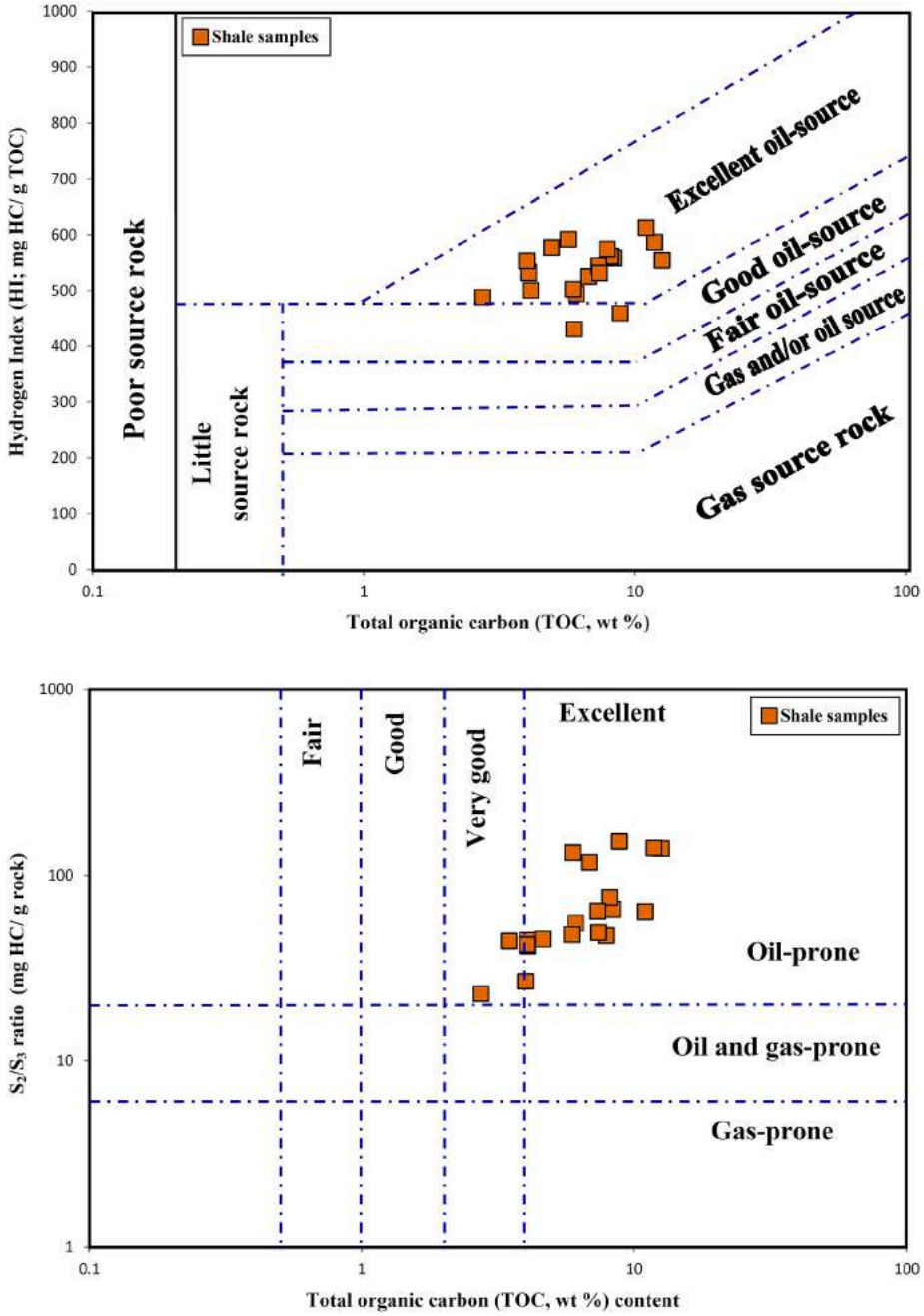

Fig. 13. Geochemical correlations between TOC content and Rock-Eval data (the HI and S_2/S_3 parameters), implying that the Madbi shales are mainly oil-prone source rocks (Gharib et al., 2021).

modified Van Krevelen diagram of HI and OI (Fig. 12a). This interpretation of the bulk Type II kerogen is compatible with the correlation between HI and T_{max}, which shows that the kerogen type mainly fell into Type II at the early stage of oil window maturity (Fig. 12b). The dominant presence of Type II kerogen that derived from the chemical kerogen-derived is generally consistent with the kerogen microscopy observed in the Madbi shale samples from the close location of the Kharir oilfield (Fig. 1B), where the Type II kerogen exhibited significant amounts of *telalginite* and *lamalginite* algae with little spores and pollens derived from plants (Fig. 9). Therefore, based on the chemical and petrological characterization of the kerogen, it is expected that the shale intervals within the Madbi Formation can generate a higher volume of oil. The high oil generative potential from the organic-rich Madbi shale sediments is inferred based on the geochemical correlation between the TOC content and pyrolysis parameters such as HI and S_2/S_3 (Fig. 13a, 13b). This potential is also verified by the composition of the free bitumen in the organic-rich Madbi shale sediments, which shows highly abundant aliphatic compounds (up to 58%) and significant amounts of aromatic and polar materials (Table 2). Thus, the generation potential of paraffinic oil from the investigated shale samples is inferred (Fig. 14).

However, the kerogen composition and classification data are inadequate to establish the true oil generation potential and should be complemented with the thermal maturity data sets. In this regard, the thermal alteration of organic matter within the analyzed Madbi shale unit was investigated through multi optical and geochemical gauges such as %VRo, T_{max}, PI, and biomarker ratios (as shown in Tables 1-3).

The measured vitrinite reflectance (%VRo) under a reflected light microscope is the most reliable maturity indicator and provides valuable

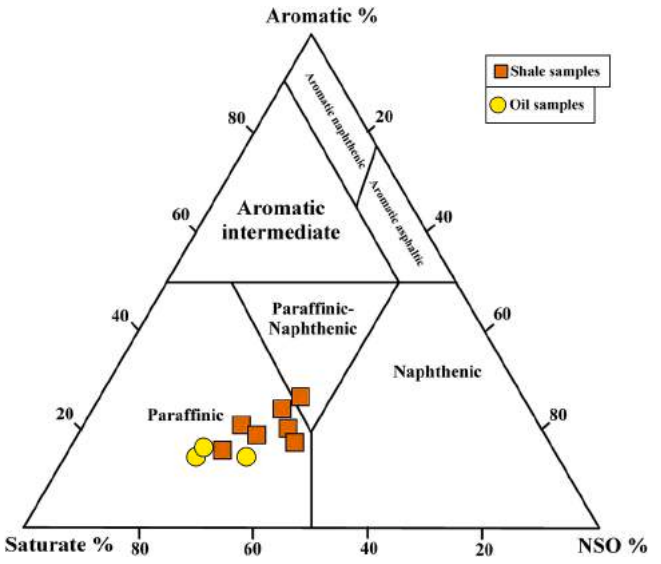

Fig. 14. Ternary diagram showing the gross composition (saturated hydrocarbons, aromatic hydrocarbons, and resins-plus-asphaltenes) of identified crude oils and bitumen extracted in the Madbi shale samples ().
Adapted from Tissot and Welte, 1984

information about the maturation level of organic matter and evolution of the petroleum generation capacity (Sweeney and Burnham, 1990; Waples, 1994). In this regard, the analyzed Madbi shale samples in the studied Sunah-1 well reached a low maturity level, consistent with the early-mature stage of the oil-generation window, as indicated from relatively low VR values of 0.63–0.73 %Vro (Table 4).

The T_{max} values were measured during the pyrolysis analysis and range from 432 °C to 444 °C (Table 1), confirming that datasets lie in the early-mature stage of the oil window (Fig. 15a). The thermal maturity of the organic matter from T_{max} data is also consistent with the PI data (ranging from 0.09 to 0.12; Table 1) and shows that the investigated Madbi shale samples are mainly early-mature source rocks (Fig. 15b).

Moreover, various biomarker fractions are also employed to evaluate the thermal maturation of organic matter. The study used the dissemination of steranes and hopanes within the saturated HC fraction of the investigated shale rock samples, following Mackenzie et al. (1980) and Seifert and Moldowan (1986). The C_{32} hopane and C_{29} sterane ββ/(ββ + αα) and 20S/(20S + 20R) ratios of the examined shale samples from Madbi Formation are 0.54–0.55, 0.40–0.43, and 0.50–0.51, respectively (Table 2), revealing the low maturity of the source rock (Fig. 15c), crossing the early mature stage of the oil generation window (Fig. 15c).

So, by integrating maturity parameters, it could be concluded that most of the examined organic matter in the shale samples derived from the Madbi Formation in the Sunah well have not yet reached high oil window maturity to generate commercial quantities of oil.

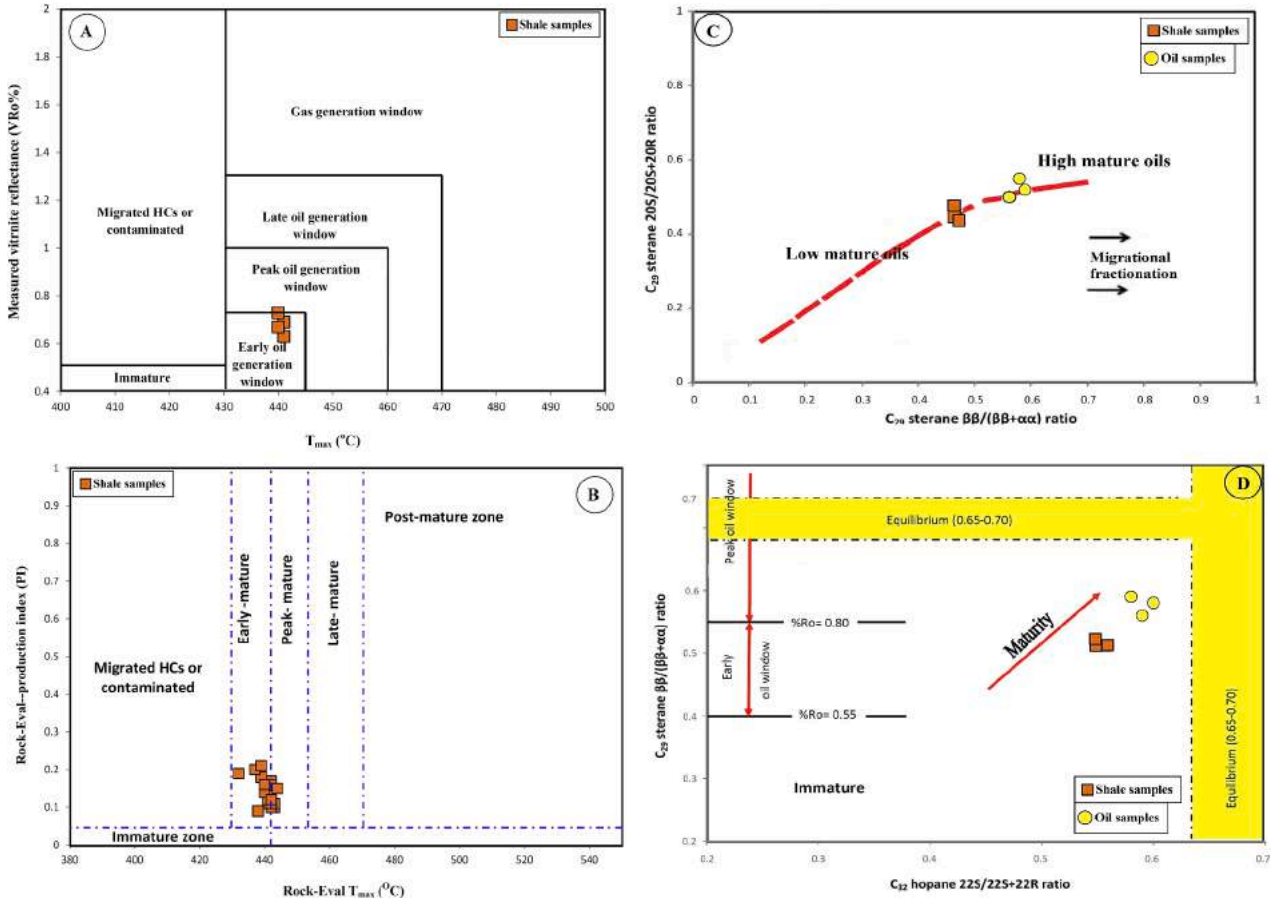

Fig. 15. Chemical and optical maturity indicators of the analyzed Madbi shale rock and oil samples from Sunah Well in the Sunah Oilfield: (a) pyrolysis T_{max} versus measured vitrinite reflectance (VRo%), (b) pyrolysis T_{max} versus production index (PI), (c) C_{29} sterane 20S/(20S + 20R) versus ββ/(ββ + αα), and (d) C_{32} hopane 22S/(22S + 22R) versus C_{29} sterane ββ/(ββ + αα), indicating that the oil are more mature that the Madbi shale samples [interpretation based on Waples and Machihara (1991) and Peters and Moldowan (1993)].

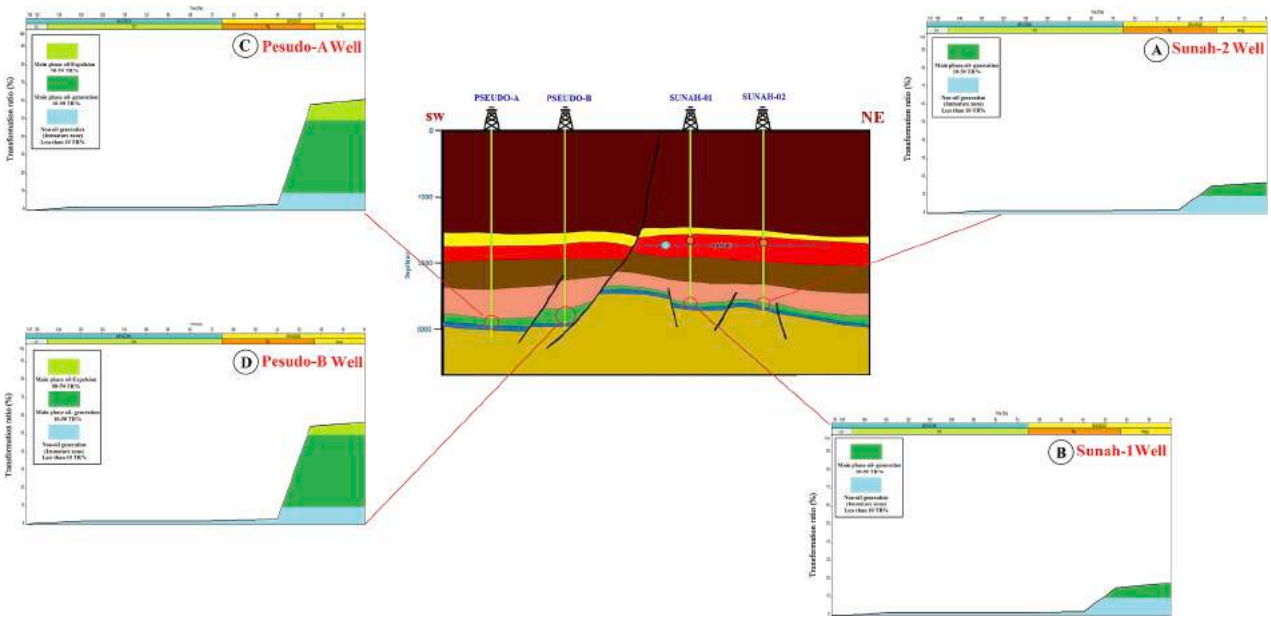

Fig. 16. Modelled transformation ratio with age for the Madbi source rock set in the four well locations across seismic interpretation in the Sunah Oilfield.

5.3. Oil characterization, classification, and geochemical correlations

The geochemical results of inorganic elements and organic biomarkers as well as isotope compositions were used to characterize and classify the analyzed oils and thus identify factors of oil–oil and oil–source rock correlations.

The physical properties reveal that the majority of the examined oil samples are light oils, with API gravity values of up to 32.6° (Table 1). Therefore, they are naturally occurring (not yet biodegraded) crude oils, as biodegraded oils have API gravity values of less than 23° (Wang et al., 2021). This finding is verified by the dominance of saturated HC in these oil samples that are greater than 50% in volume (Table 1). The absence of biodegradation in the studied oil samples is also supported by relatively higher saturate/aromatic ratio of more than 3 (3.91–4.39), as shown in Table 2. However, the dominance of saturated HC indicates that these studied oils are mainly classified as paraffinic oils, with little composition as paraffinic-naphthenic oils (Fig. 14), according to a ternary diagram of Tissot and Welte (1984).

In addition to the physical properties and the chemical compositions, the full complement of lighter and heavier *n*-alkanes ranging between C_{12} and C_{36} and isoprenoids (Fig. 5a), with a straight chromatogram baseline, further refers to non-biodegradation in these oils (Connan, 1984; Larter et al., 2005).

The *n*-alkane distributions of the oils are concentrated by short-and middle chain *n*-alkanes compared to the long-chain *n*-alkanes (Fig. 5a), indicating a mixture of marine organic matter and little terrigenous input, with a major contribution of algal and microbial organic matter input (Didyk et al., 1978; Peters et al., 2005). The carbon isotope values of saturated and aromatic hydrocarbon fractions of the oils are consistent with the origin of marine organic matter (Fig. 4).

In addition, the relatively highest values of Pr/Ph, Pr/*n*-C_{17}, and Ph/*n*-C_{18} ratios (Table 3) further correspond to crude oils originated from source rock that contains mixed marine and terrestrial organic matter and deposited under relatively low reducing (suboxic) environmental conditions (Fig. 8a and 8b). The suboxic environmental conditions for the potential source rock are also demonstrated by the V/N ratio values of the oils between 1.03 and 1.12 (Table 2). This interpretation is corroborated by the distribution of the hopanes and tricyclic terpanes (Table 3). The marine environment of the potential source rocks for the studied oils is implied by the relationship between the DBT/Phen, Pr/Ph, $C_{31}R/C_{30}H$, and C_{26}/C_{25} tricyclic terpane ratios (Fig. 8c and 8d). Moreover, the high marine microorganism contributions of phytoplankton algae and bacteria are also compatible with the regular sterane distributions (Fig. 10).

As per the previously discussed results of inorganic geochemical elements and physical properties, the genetic link between the studied oil samples themselves and their corresponding source rocks was correlated.

The oil samples had very similar features, including their oil compositions and molecular and isotopic characteristics (Figs. 4, 8, 10, and 14). The environment-based biomarkers proposed that the oil samples collected from different Jurassic and Cretaceous reservoirs could have been generated from the same source rock, which is characterized by clay-rich rock and a marine depositional setting. These characteristics are consistent with the Madbi organic-rich shale samples as demonstrated by the environment-based biomarkers and isotopic characteristics (Figs. 4, 8, and 10). Therefore, the organic matter-rich Madbi shales are considered to be the main source rocks of the most oils in the Sunah oilfield.

However, the maturity ratios of aliphatic and aromatic biomarkers show a clear differentiation between the extracted Madbi shale samples and the oils from the Sunah well (Table 3). For example, biomarker maturity ratios and parameters of the aliphatic hydrocarbon and aromatic fractions, including C_{32} hopane and C_{29} sterane ββ/(ββ + αα) and 20S/(20S + 20R), and moretane/C_{30} hopane (CM_{30}/C_{30}) ratios and calculated reflectance (VRc) were applied in determining the maturity of both extracted shale samples and oils (e.g., Seifert and Moldowan, 1986; Mackenzie et al., 1980; Radke et al., 1986).

These maturity ratios of aliphatic and aromatic biomarkers of the extracted Madbi shale from structural heights indicate that the oils are slightly more mature than the extracts (Table 3). The oil samples reached a peak-oil window, with high C_{32} hopane and C_{29} sterane ββ/(ββ + αα) and 20S/(20S + 20R) ratios (Fig. 15c and 15d) and VRc values between 0.81% and 0.82% (Table 3). Further, the analyzed shale samples at the early-mature of oil window achieved relatively low C_{32} hopane and C_{29} sterane ββ/(ββ + αα) and 20S/(20S + 20R) ratios (Fig. 15c and 15d) and VRc values of between 0.72% and 0.74% (Table 3). Hence, the reservoir oils in the Sunah oilfield were generated from relatively high mature Madbi source rock in a known deeper location of the oilfield. This finding is confirmed by the burial and thermal maturity models (Fig. 7). Based on the models of burial/thermal history, the Madbi source rock in the known deeper location of Pseudo A

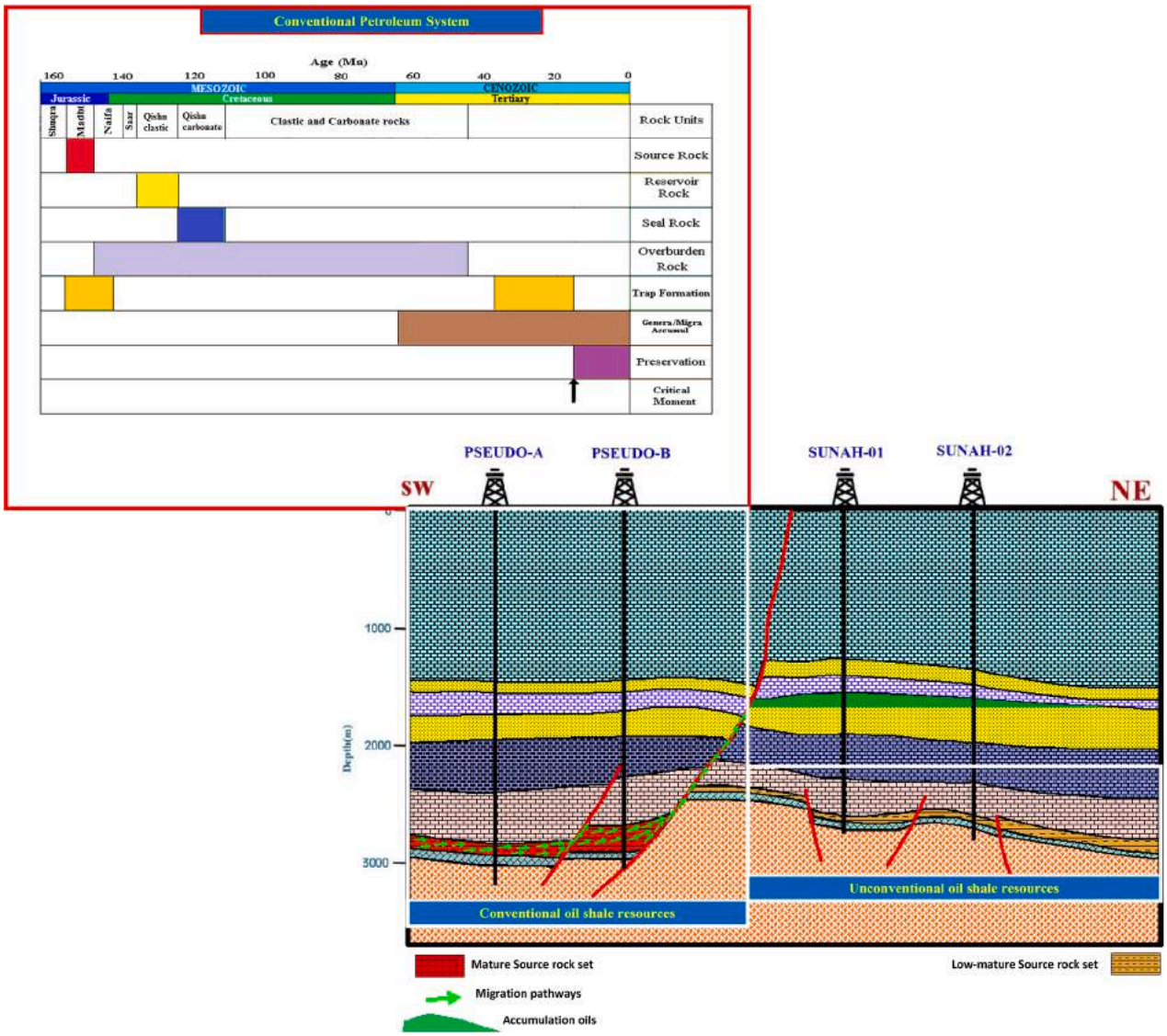

Fig. 17. Schematic geological cross section in the Sunah Oilfield, shown that the Madbi source rock set in the structural highs is considered as unconventional oil potential, while the Madbi source rock set in the know deeper locations is generally consistent with the characteristics of the conventional petroleum system.

and B wells are buried deeper than those of Sunah-1 and Sunah-2 (Fig. 3) and are more thermally mature in a peak-oil window, as demonstrated from the modeled VR values of more than 0.80 EASY% Ro (Fig. 7). Therefore, the Madbi Formation is likely to be an effective oil-source rock; however, most of the oils in the Sunah oilfield were mainly generated from the relatively highly mature Madbi source rock in the known deeper location of the Pseudo A and B wells in the oilfield.

5.4. Simulating the oil generation and expulsion over time

Petroleum generation and expulsion from the Late Jurassic Madbi shale source rock over time were simulated based on the integration geochemical and optical results discussed in the previous sections in this study as well as the geological information from four wells across the seismic interpretation line in the Sunah oilfield (Fig. 3) incorporated into the basin modeling.

The Madbi source rock is rich in planktonic-bacterial organic matter, as mentioned in the geochemical results above, and is comprised of a Type II kerogen (Fig. 12). Therefore, the petroleum generation and expulsion over time were predicted from the kerogen conversion ratios (TR %) based on kinetic data of Tissot et al. (1987) for Type II kerogen. These TR ratios of the initial kerogen cracking to oil and then expulsion of oil through the Madbi source rock set were expressed from the computed EASY% Ro values (Fig. 7).

The burial/maturity models are compatible with the kinetic data of Type II kerogen and show that the Madbi source rock set in the highest structure area (i.e., Sunah-1 and Sunah-2 wells) reached low TR% of 10–17% during the early Oligocene (31 Ma) to today (Fig. 17a and 17b). Consequently, the organic-rich intervals have not yet generated commercial oils. In contrast, the Madbi source rock in the lowest structure area (i.e., Pseudo-A and Pseudo-B wells) has a high conversion ratio of more than 50% (Fig. 17c and 17d). Here, the organic-rich intervals reached a conversion ratio of 10–50% and began to generate commercial oils during the late Eocene to early Oligocene (Fig. 17c and 17d). Additionally, the Madbi source rock reached the highest TR ratio of up to 50% during the early Oligocene (27–26 Ma) to date (Fig. 17c and 17d), resulting in the generation of large amounts of oil. The large amounts of oil generated during the late Eocene to early Oligocene led to high pressures; thus, the source rock set expelled oils during the early Oligocene and continues to do so today (Fig. 17c and 17d). Furthermore, the high conversion ratios of more than 50% possibly explain that the accumulated oils in the Sunah oilfield were primarily migrated from the

source rock set in the lowest structure area (Pseudo-A and Pseudo-B wells) and then trapped in the reservoir rocks.

5.5. Implications on conventional and unconventional resources potential

In the last 20 years, the Say'un–Masilah Basin has been explored and developed for petroleum activities requiring conventional petroleum resources. On the basis of the oil exploration results, discoveries in the Say'un–Masilah Basin focused on Mesozoic units indicated that the Madbi Formation deposited during Late Jurassic is a main conventional petroleum resource and contributed to generating most of the oils accumulated in the basin (e.g., Al Areeq and Maky, 2015 Hakimi et al., 2011). However, the quality of the increasingly produced oil from the conventional reserves in the basin has been declining. Therefore, exploration and research on unconventional petroleum resources have significantly increased in recent times. In this regard, the potential of conventional and unconventional resources in the basin needed to be established and clarified. Hence, the integrated geochemical and basin model results were highlighted to understand the conventional and unconventional resources for the exploration of the remaining petroleum in the basin.

The current study identifies the characterization and effectiveness of the organic-rich shale within the Late Jurassic Madbi Formation in the Sunah oilfield and reveals it as both a conventional and unconventional oil potential. The potential of conventional and unconventional oil resources also laterally changed from one well site to another.

The conventional oil resource potential is better in the known deeper area (Pseudo-A and Pseudo-B wells), and the unconventional oil resource potential is better in the highest structure area (Sunah-1 and Sunah-2 wells), as shown in Fig. 17. This difference in the potential of conventional and unconventional oil resources is attributed to the thermal maturity of the organic matter, which is vertically affected by the temperature distributions with varying burial depths.

The organic-rich shales within the Madbi Formation in the highest structure area (Sunah-1 and Sunah-2 wells) are considered to be the unconventional oil resource potential in the Sunah oilfield and are characterized by a high TOC of up to 12%, where the Madbi source rock reached the early-mature stage of the oil generation window (Fig. 7), with low values of VR (0.63–0.73%). This high organic content of Madbi shales, combined with their relatively low maturity in the oil generation window, indicates that the Madbi shales may have generated certain amounts of oil but have not yet generated and then expelled commercial oils, as demonstrated by the low kerogen conversion ratios of 10–17 TR % (Fig. 16a and 16b). These low ratios of kerogen conversion may have resulted in the retention of more oil potential and could be pyrolyzed to release significant amounts of oil using unconventional artificial techniques.

In addition, the geochemical oil-source rock correlation proposes that the oil's regional distribution in the Sunah oilfield was mainly derived from the mature Madbi shales. And so, the Madbi Formation in the Sunah oilfield is also likely to be part of the main conventional petroleum source rock. The conventional oil potential occurs in the known deeper area (Fig. 17), where the Madbi source rock has reached peak-oil window maturity (Fig. 7), and a high kerogen conversion ratio of more than 50% (Fig. 16c and 16d) generates and expels large amounts of oil. Given this, the current conventional petroleum potential study examines the match between the Madbi source rock, reservoir, seal rock, timing of generation, migration, and trap formation in the Sunah oilfield (Fig. 17).

Within the Sunah oilfield, the Late Jurassic Madbi Formation acts as the source rock with the most significant generation. Since there also is a positive association between oil production and the source rock (Figs. 4, 8, and 10), the Madbi source rock set in a known deeper area (Pseudo-A and Pseudo-B wells) is generally consistent with the characteristics of a conventional petroleum system (Fig. 17). Herein, this conventional petroleum system, including elements and processes of the petroleum generation and migration over geological time, was described based on the integration of geological information with the geochemical and basin model results of the current study.

The petroleum system examined during this study reveals that the oil generation initiating from the Late Jurassic Madbi shales set in the known deeper area, which reached the peak of oil-window maturity during the early Paleocene to late Oligocene (Fig. 7), resulted in the generation of significant amounts of oil with a high conversion ratio of up to 50% (Fig. 16c and 16d). The maximum amounts of oil generation, with a high conversion ratio of up to 50%, may have also caused high pressure through the source rock set, thereby contributing to oil expulsion. The burial/thermal history models also explain the oil expulsion from the Madbi source rock initiated during the early Oligocene and continuing to the present day (Fig. 16c and 16b). Whereas the migration of the hydrocarbons to the shallow Qishn reservoir rocks started during the same period as a result of the opening of the Red Sea–Gulf of Aden rift system during the Oligo-Miocene, as reported previously (Redfern and Jones, 1995; Bosworth et al., 2005; As-Saruri et al., 2010). The volumes of oil eventually moved up along vertical migration paths and across the normal fault systems of the Oligo-Miocene and then accumulated in the reservoir sandstone unit of the Qishn Formation (Fig. 17). The Qishn reservoir sandstone unit was covered by the carbonate and shale intervals of the Cretaceous Qishn Formation as regional seal rocks (Fig. 17). However, the Miocene appears to be the critical moment for the Madbi conventional petroleum system, as shown in Fig. 17.

6. Conclusions

Conventional and unconventional petroleum potentials of the organic-rich shale intervals within the Late Jurassic Madbi Formation in the Sunah oilfield in the Say'un–Masilah Basin were performed using integration organic geochemical and basin modeling techniques. The following conclusions were drawn from the results and are summarized below.

- Madbi shales from structural heights in the Sunah Oilfield are likely to be favorable source rocks for petroleum generation, as implied by the high TOC of up to 12 wt% and petroleum potential yields of up to 70.43 mg HC/g rock.
- Madbi shales contain large amounts of marine-derived organic matter, primarily phytoplankton algae and Type-II kerogen, based on high HI values of 431–613 HC/g TOC. Thus, they are highly oil-prone source rocks.
- Madbi shales were deposited under relatively reducing environmental conditions, which contribute to the preservation of organic matter.
- Biomarker and carbon isotope data, coupled with basin models, confirm that the oils accumulated in the Sunah oilfield were mainly generated and expelled from the mature Madbi source rock set in known deeper locations of the oilfield, with high conversion ratios of more than 50%.
- Basin models also indicate that the Madbi source rock in the Sunah oilfield has both conventional and unconventional petroleum potentials.
- Conventional and unconventional petroleum potentials are affected by the burial temperature distributions and laterally changed from one site to another along the oilfield.
- Unconventional petroleum potential mainly occurred in the highest structure areas of the oilfield, where the Madbi source rock exhibits low oil-window maturity and 10–17% kerogen cracking, thereby resulting in the retention of more oil potential that could be to produce significant amounts of oil using unconventional techniques.
- The Madbi source rock set in the known deeper locations reached the peak-mature stage of the oil window and a high conversion ratio of more than 50%, consistent with the characteristics of the

conventional petroleum potential, including the Madbi source rock, reservoir, seal rock, timing of generation, migration, and trap formation.

CRediT authorship contribution statement

Mohammed Hail Hakimi: Conceptualization, Data curation, Formal analysis, Investigation, Project administration, Writing – original draft. **Mikhail A. Varfolomeev:** Funding acquisition, Supervision. **Ali Y. Kahal:** Funding acquisition, Writing – review & editing. **Abbas F. Gharib:** Software, Funding acquisition, Writing – review & editing. **Fahad Alshehri:** Funding acquisition, Writing – review & editing. **Afikah Rahim:** Software, Writing – review & editing. **Hussain J. Al Faifi:** Funding acquisition, Writing – review & editing. **Ameen A. Al-Muntaser:** Software, Writing – review & editing. **Saleh Qaysi:** Funding acquisition, Writing – review & editing. **Karem Abdelmohsen:** Writing – review & editing.

Declaration of Competing Interest

The authors declare that they have no known competing financial interests or personal relationships that could have appeared to influence the work reported in this paper.

Acknowledgments

The first author acknowledges the Petroleum Exploration and Production Authority (PEPA), Republic of Yemen for supplying the geochemical materials. This work was also supported by the Ministry of Science and Higher Education of the Russian Federation under agreement No. 075-15-2020-931 within the framework of the development program for a world-class Research Center “Efficient development of the global liquid hydrocarbon reserves”. The authors extend their sincere appreciation to the Researchers Supporting Project number (RSP-2021/327), King Saud University, Riyadh, Saudi Arabia. We also are grateful to the Guest Editors board members Dr. Ahmed E. Radwan, Prof. Dr. Abdulrahman. S. Alsharhan and Dr. David A.Wood for organizing this special issue in the Journal of Asian Earth Sciences. The constructive comments by anonymous reviewers have improved the original manuscript are gratefully acknowledged.

References

Al-Areeq, N.M., 2018. Petroleum source rocks characterization and hydrocarbon generation. In: Zoveidavianpoor, M. (Ed.), Recent Insights in Petroleum Science and Engineering, INTEQ publisher, pp. 1–29. https://doi.org/10.5772/intechopen.

Al Areeq, N.M., Maky, A.F., 2015. Organic geochemical characteristics of crude oils and oil-source rock correlation in the Sunah oilfield, Masila Region, Eastern Yemen. Mar. Pet. Geol. 63, 17–27.

Al-Areeq, N.M., Elhossainy, M.M., Salman, A.M., 2020. Sequence stratigraphic architecture of the Upper Jurassic-Lower Cretaceous deposits in the Sayun-Masilah Basin, Yemen: A case study from Masilah oilfields. J. Asian Earth Sci. 192, 104287.

Al-Johi, A., Ibrahim, E., Al Faifia, H.J., Kinawy, M.M., Al Arifia, N.S., Lashin, A., 2019. Investigating deep geological reservoirs using seismic reflection and well logs, Tawila oil field, Yemen: Implications for structural setting and reservoir properties. J. Petrol. Sci. Eng. 176, 1018–1040.

Allen, P.A., Allen, J.R., 1990. Basin Analysis Principles and Applications. Blackwell Scientific Publications, Oxford, pp. 1–642.

Allen, P.A., Allen, J.R., 2005. Basin Analysis: Principles and Applications. Blackwell, Oxford, p. 549.

Ardakania, O.H., Sanei, H., Ghanizadeh, A., McMechan, M., Ferric, F., Clarkson, C.R., 2017. Hydrocarbon potential and reservoir characteristics of Lower Cretaceous Garbutt Formation, Liard Basin Canada. Fuel 209, 274–289.

As-Saruri, M.A., Sorkhabi, R., Baraba, R., 2010. Sedimentary basins of Yemen: their tectonic development and lithostratigraphic cover. Arab. J. Geosci. 3, 515–527.

Beydoun, Z.R., Al-Saruri, M., Baraba, R.S., 1996. Sedimentary basins of the Republic of Yemen: their structural evolution and geological characteristics. Revue de L. Institute Francaiselu Petrole 51, 763–775.

Beydoun, Z.R., Al-Saruri, M., El-Nakhal, H., Al-Ganad, I.N., Baraba, R.S., Nani, A.S.O., Al-Aawah, M.H., 1998. International lexicon of stratigraphy, second ed., vol. 3. In: Republic of Yemen, International Union of Geological Sciences and Ministry of Oil and Mineral Resources Publication, vol. 34, pp. 245.

Bissada, K.K., 1982. Geochemical constraints on petroleum generation and migration—a review. Proc ASCOPE Conf. 81, 69–87.

Bornemann, A., Aschwer, U., Mutterlose, A.J., 2003. The impact of calcareous nannofossils on the pelagic carbonate accumulation across the Jurassic-Cretaceous boundary. Palaeogeogr. Palaeoclimatol. Palaeoecol. 199, 187–228.

Bosworth, W., Huchon, P., McClay, K., 2005. The Red Sea and Gulf of Aden Basins. J. Afr. Earth Sc. 43, 334–378.

Boutaleb, K., Baouche, R., Sadaoui, M., Radwan, A.E., 2021. Sedimentological, petrophysical, and geochemical controls on deep marine unconventional tight limestone and dolostone reservoir: Insights from the Cenomanian/Turonian oceanic anoxic event 2 organic-rich sediments, Southeast Constantine Basin, Algeria. Sed. Geol. 106072.

Brannin, J., Sahota, G., Gerdes, K.D., Berry, J.A.L., 1999. Geological evolution of the central Marib-Shabwah basin, Yemen. GeoArabia 4, 9–34.

Caineng, Z., Guosheng, Z., Zhi, Y., Shizhen, T., Lianhua, H., Rukai, Z., Xuanjun, Y., Qiquan, R., Denghua, L., Zhiping, W., 2013. Concepts, characteristics, potential and technology of unconventional hydrocarbons: On unconventional petroleum geology. Petrol. Explor. Develop. 40, 413–428.

Chakhmakhchev, A., Suzuki, N., 1995. Aromatic sulfur compounds as maturity indicators for petroleums from the Buzuluk depression, Russia. Org. Geochem. 23, 617–625.

Chandra, K., Mishra, C.S., Samanta, U., Gupta, A., Mehrotra, K.L., 1994. Correlation of different maturity parameters in the Ahmedabad-Mehsana Block of the Cambay Basin. Org. Geochemis. 21, 313–321.

Cranwell, P.A., 1977. Organic geochemistry of Cam Loch (Sutherland) sediments. Chem. Geol. 20, 205–221.

Didyk, B.M., Simoneit, B.R.T., Brassell, S.C., Eglinton, G., 1978. Organic geochemical indicators of palaeoenvironmental conditions of sedimentation. Nature 272, 16–222.

Espitalie, J., Laporte, L., Madec, M., Marquis, F., Leplate, P., Pault, J., Boutefeu, A., 1977. Methode rapid de caracterisation des rocks meres, deleur potential petrolier et leurdegre devolution. Rev. Inst. Fr. Petrol. 32, 23–42.

Espitalie, J., Deroo, G., Marquis, F., 1985. La pyrolyse Rock-Eval et ses applications. Partie 1. Revue de 1’Lnstitut Francois du Petrole 40, 563–579.

Galarraga, F., Llamas, J.F., Martinez, A., Martinez, M., Marquez, G., 2008. V/Ni ratio as a parameter in palaeoenvironmental characterization of non-mature medium-crude oils from several Latin American basins. J. Petrol. Sci. Eng. 61, 9–14.

Gelpi, E., Schneider, H., Mann, J., Oro, J., 1970. Hydrocarbons of geochemical significance in microscopic algae. Phytochemistry 9, 603–612.

Gharib, A.F., Özkan, A.M., Hakimi, M.H., Zainal Abidin, N., Lashin, A., 2021. Integrated geochemical characterization and geological modeling of organic matter-rich limestones and oils from Ajeel Oilfield in Mesopotamian Basin, Northern Iraq. Marine Petrol. Geol. 126, 104930.

Gürgey, K., 1999. Geochemical characteristics and thermal maturity of oils from the Thrace Basin (western Turkey) and western Turkmenistan. J. Pet. Geol 22, 167–189.

Hadad, Y.T., Mohammed Hail Hakimi, M.H., Abdullah, A.H., Kinawy, M., El Mahdy, O., Lashin, A., 2021. Organic geochemical characteristics of Zeit source rock from Red Sea Basin and their contribution to organic matter enrichment and hydrocarbon generation potential. J. Afric. Earth Sci. 177.

Hakimi, M.H., Abdullah, W.H., Shalaby, M.R., 2010. Source rock characterization and oil generating potential of the Jurassic Madbi Formation, onshore East Shabowah oilfields, Republic of Yemen. Org Geochem. 41, 513–521.

Hakimi, M.H., Abdullah, W.H., Shalaby, M.R., 2011. Organic geochemical characteristics of crude oils from the Masila Basin, eastern Yemen. Org Geochem. 42, 465–476.

Hakimi, M.H., Abdullah, W.H., Shalaby, M.R., 2012. Molecular composition and organic petrographic characterization of Madbi source rocks from the Kharir Oilfield of the Masila Basin (Yemen): palaeoenvironmental and maturity interpretation. Arab. J. Geosci. 5, 817–831.

Hakimi, M.H., Abdullah, W.H., Hersi, O.S., Lashin, A.A., El Alfye, M.M., Makeen, Y.M., Kinawy, M.M., Hatem, B.A., 2020a. Organic geochemistry of the Early Cretaceous shales, Saar Formation in the East Shabwah oil fields, onshore Masila Basin of eastern Yemen. J. Petrol. Sci. Eng. 179, 394–409.

Hakimi, M.H., Abdullah, W.H., Lashin, A.A., El-Khedr, H.I., Makeen, Y.M., 2020b. Hydrocarbon Generation Potential of the Organic-Rich Naifa Formation, Say’un–Masila Rift Basin, Yemen: Insights from Geochemical and Palynofacies Analyses. Nat. Resour. Res. 29, 2687–2715.

Haitham, F.M., Nani, A.S.O., 1990. The Gulf of Aden rift: hydrocarbon potential of the Arabian sector. J. Pet. Geol 13, 211–220.

Hanson, A.D., Zhang, S.C., Moldowan, J.M., Liang, D.G., Zhang, B.M., 2000. Molecular organic geochemistry of the Tarim basin, NW China. Am. Assoc. Pet. Geol. Bull. 84, 1109–1128.

Hantschel, T., Kauerauf, A.I., 2009. Fundamentals of Basin and Petroleum Systems Modeling: Integrated Exploration Systems GmbH. Schlumberger Company, Springer-Verlag Berlin Heidelberg. https://doi.org/10.1007/978-3-540-72318-9.

He, S., Middleton, M., 2002. Heat flow and thermal maturity modelling in the northern carnarvon basin, north west shelf, Australia. Mar. Petrol. Geol. 19, 1073–1088.

Hughes, W.B., Holba, A.G., Dzou, L.I.P., 1995. The ratios of dibenzothiophene to phenanthrene and pristane to phytane as indicators of depositional environment and lithology of petroleum source rocks. Geochim. Cosmochim. Acta 59, 3581–3598.

Jarvie, D.M., 1991. Total organic carbon (TOC) analysis. In: Merrill, R.K. (Ed.), Treatise of Petroleum Geology: Handbook of Petroleum Geology, Source and Migration Processes and Evaluation Techniques. American Association of Petroleum Geologists, Tulsa, pp. 113–118.

Jarvie, D.M., Claxton, B.L., Henk, F., Breyer, J.T., 2001. Oil and shale gas from the Barnett Shale, Fort Worth basin, Texas. AAPG National Convention, June 3-6, 2001, Denver, CO. AAPG Bull. 85, 13 (Supplement), A100.

Katz, B., Lin, F., 2014. Lacustrine basin unconventional resource plays: key differences. Mar. Pet. Geol. 56, 255–265.

Katz, B., Lin, F., 2021. Consideration of limitations of thermal maturity with respect to vitrnite reflectance, Tmax and other proxies. AAPG 105, 695–720.
Lachenbruch, A., 1970. Crustal temperature and heat productivity: implications of the linear heat flow relation. J. Geophys. Res. 75, 3291–3300.
Large, D.J., Gize, A.P., 1996. Pristane/phytane ratios in the mineralized Kupferschiefer of the Fore-Sudetic Monocline, southwest Poland. Ore Geol. Rev. 11, 89–103.
Larter, S.R., Head, I.M., Huang, H., Bennett, B., Jones, M., Aplin, A.C., Murray, A., Erdmann, M., Wilhelms, A., di Primio, R., 2005. Biodegradation, gas destruction and methane generation in deep subsurface petroleum reservoirs: an overview. In: Dore, A.G., Vining, B. (Eds.), Petroleum Geology: Northwest Europe and Global Perspectives: Proceedings of the 6th Petroleum Geology Conference, Geological Society, London, pp. 633–640.
Lewan, M.D., Kotarba, M.J., Curtis, J.B., Wieclaw, D., Kosakowski, P., 2006. Oil generation kinetics for organic facies with Type-II and -IIS kerogen in the Menilite Shales of the Polish Carpathians. Geochim. Cosmochim. Acta 70, 3351–3368.
Mackenzie, A.S., Patience, R.L., Maxwell, J.R., Vandenbroucke, M., Durand, B., 1980. Molecular parameters of maturation in the Toarcian shales, Paris Basin, France—I. Changes in the configurations of acyclic isoprenoid alkanes, steranes and triterpanes. Geochim. Cosmochim. Acta 44, 1709–1721.
Makeen, Y.M., Abdullah, W.H., Hakimi, M.H., Mustapha, K.A., 2015. Source rock characteristics of the lower cretaceous Abu Gabra formation in the Muglad Basin, Sudan, and its relevance to oil generation studies. Mar. Pet. Geol. 59, 505–516.
Makeen, Y.M., Abdullah, W.H., Pearson, M.J., Hakimi, M.H., Elhassan, O.M.A., Hadad, Y. T., 2016. Thermal maturity history and petroleum generation modelling for the lower Cretaceous Abu Gabra Formation in the Fula sub-basin, Muglad basin. Sudan. Mar. Petrol. Geol. 75, 310–324.
Makeen, Y.M., Abdullah, W.H., Abdul Ghofur, M.N., Ayinla, H.A., Hakimi, M.H., Shan, X., Mustapha, K.A., Shuib, M.K., Liang, Y., Zainal Abidin, N.S., 2019. Hydrocarbon Generation Potential of Oligocene Oil Shale Deposit at Onshore Penyu Basin, Chenor, Pahang, Malaysia. Energy Fuels 33, 89–105.
Mansour, A., Wagreich, M., Gentzis, T., Ocubalidet, S., Tahoun, S.S., Elewa, A.M.T., 2020. Depositional and organic carbon-controlled regimes during the Coniacian-Santonian event: First results from the southern Tethys (Egypt). Mar. Pet. Geol. 115, 104285.
Mountain, G., Prell, W., 1990. A multiphase plate tectonic history of the southeast continental margin of Oman. Geol. Soc. Lond. Spec. Publ. 49, 725–743.
Mukhopadhyay, P.K., Wade, J.A., Kruge, M.A., 1995. Organic facies and maturation of Jurassic/Cretaceous rocks, and possible oil-source rock correlation based on pyrolysis of asphaltenes, Scotion Basin, Canada. Org Geochem. 22, 85–104.
Orr, W.L., 2001. Evaluating kerogen sulfur content from crude oil properties. In: Isaacs, C.M., Rullkotter, J. (Eds.), The Monterey Formation from Rocks to Molecules. Columbia University Press, New York, pp. 348–367.
Peters, K., Cassa, M., 1994. Applied source rock geochemistry. In: Magoon, L.B., Dow, W. G., editors. The Petroleum System from Source to Trap. AAPG Memoir, vol. 60, pp. 93–117.
Peters, K.E., Moldowan, J.M., 1993. The Biomarker Guide: Interpreting Molecular Fossils in Petroleum and Ancient Sediments: Englewood Cliffs. Prentice Hall, New Jersey, p. 363.
Peters, K.E., Walters, C.C., Moldowan, J.M., 2005. The Biomarker Guide 2: Biomarkers and Isotopes in Petroleum Exploration and Earth Zhistory, second ed. Cambridge University Press, Cambridge, United Kingdom, p. 704.
Qadri, S.M.T., Shalaby, M.R., Islam, M.A., Hoon, L.L., 2016. Source Rock Characterization and hydrocarbon generation modeling of the Middle to Late Eocene Mangahewa Formation in Taranaki Basin, New Zealand. Arab. J. Geosci. 9, 559.
Qadri, S.M.T., Islam, M.A., Shalaby, M.R., Ali, S.H., 2021. Integration of 1D and 3D modeling schemes to establish the Farewell Formation as a self-sourced reservoir in Kupe Field, Taranaki Basin, New Zealand. Front. Earth Sci. 15, 631–648.
Radke, M., Welte, D.H., Willsch, H., 1986. Maturity parameters based on aromatic hydrocarbons: Influence of the organic matter type. Org Geochem. 10, 51–63.
Radwan, A.E., Rohais, S., Chiarella, D., 2021. Combined stratigraphic-structural play characterization in hydrocarbon exploration: A case study of Middle Miocene sandstones, Gulf of Suez basin, Egypt. J. Asian Earth Sci. 104686.
Redfern, P., Jones, J.A., 1995. The interior rifts of Yemen–701 analysis of basin structure and stratigraphy in a regional plate tectonic context. Basin Res. 7, 337–356.
Rowland, S., Rockey, C., Allihaibi, S.S., Wolff, G.A., 1993. Incorporation of Sulfur into Phytol Derivatives during Simulated Early Diagenesis. Org Geochem. 20, 1–5.
Sarki Yandoka, B.M., Abdullah, W.H., Abubakar, M.B., Hakimi, M.H., Mustapha, K.A., Adegoke, A.K., 2015. Organic geochemical characteristics of Cretaceous Lamja Formation from Yola Sub-basin, Northern Benue Trough, NE Nigeria: implication for hydrocarbon-generating potential and paleodepositional setting. Arab. J. Geosci. 8, 7371–7386.
Schwark, L., Empt, P., 2006. Sterane biomarkers as indicators of Palaeozoic algal evolution and extinction events. Palaeogeogr. Palaeoclimatol. Palaeoecol. 240, 225–236.
Seifert, W.K., Moldowan, J.M., 1986. Use of biological markers in petroleum exploration. In: Johns, R.B., (Ed.), Amsterdam: Methods in Geochemistry and Geophysics Book Series, vol. 24, pp. 261–290.
Shalaby, M.R., Hakimi, M.H., Abdullah, W.H., 2011. Geochemical characteristics and hydrocarbon generation modeling of the Jurassic source rocks in the Shoushan Basin, north Western Desert. Egypt. Mar. Petrol. Geol. 28, 1611–1624.
Sofer, Z., 1984. Stable carbon isotope compositions of crude oils: application to source depositional environments and petroleum alteration. Am. Assoc. Petrol. Geol. Bullet. 68, 31–49.
Sweeney, J.J., Burnham, A.K., 1990. Evaluation of a simple model of vitrinite reflectance based on chemical kinetics. Am. Assoc. Pet. Geol. Bull. 74, 1559–1570.
Taylor, G., Teichmüller, M., Davis, A., Diessel, C., 1998. Organic Petrology.
Ten Haven, H.L., de Leeuw, J.W., Rullkötter, J., Damsté, J.S.S., 1987. Restricted utility of the pristane/phytane ratio as a palaeoenvironmental indicator. Nature 330, 641–643.
Tissot, B.P., Welte, D.H., 1984. Petroleum Formation and Occurrence, second ed. Springer Verlag, Berlin., p. 699
Tissot, B.P., Pelet, R., Ungerer, P.H., 1987. Thermal history of sedimentary basins, maturation indices and kinetics of oil and gas generation. Am. Assoc. Pet. Geol. Bull. 71, 1445–1466.
Tserolas, P., Maravelis, A.G., Tsochandaris, N., Pasadakis, N., Zelilidis, A., 2019. Organic geochemistry of the Upper Miocene-Lower Pliocene sedimentary rocks in the Hellenic Fold and Thrust Belt, NW Corfu island, Ionian sea, NW Greece. Mar. Pet. Geol. 106, 17–29.
Tyson, R.V., 1995. Sedimentary Organic Matter—Organic Facies and Palynofacies. Chapman & Hall, London, p. 615.
Wang, W., Wang, T., Li, M., Mao, F., Liu, J., Xiao, H., Lai, H., Ai, X., 2021. The origins of biodegraded oils in sandstone reservoirs in the Termit Basin. J. Petrol. Sci. Eng. 207, 109130.
Waples, D.W., Machihara, T., 1991. Biomarkers for Geologists – A Practical Guide to the Application of Steranes and Triterpanes in Petroleum Geology: Association of Petroleum Geologists, Methods in Exploration No. 9, 91 p.
Welte, D.H., Horsfield, B., Baker, D.R., 2012. Petroleum and Basin Evolution: Insights from Petroleum Geochemistry, Geology and Basin Modeling. Springer, Berlin Heidelberg.
Wenger, L.M., Davis, C.L., Isaksen, G.H., 2002. Multiple controls on petroleum biodegradation and impact on oil quality. Reservoir Evaluat. Eng. 5, 375–383.
Wu, J., Liang, C., Hu, Z.Q., Yang, R.C., Xie, J., Wang, R.Y., Zhao, J.H., 2019. Sedimentation mechanisms and enrichment of organic matter in the Ordovician Wufeng Formation-Silurian Longmaxi Formation in the Sichuan Basin. Mar. Petrol. Geol. 101, 556–565.
Zumberge, J.E., 1987. Terpenoid biomarker distributions in low maturity crude oils. Org Geochem. 11, 479–496.
Hughes Clarke, M.W., 1988. Stratigraphy and rock-unit nomenclature in the oil producing area of Interior Oman. J. Petrol. Geol. 11, 5–60.
Hakimi, M.H., Abdullah, W.H., Alqudah, M., Makeen, Y.M., Mustapha, K.A., 2016. Organic geochemical and petrographic characteristics of the oil shales in the Lajjun area, Central Jordan: Origin of organic matter input and preservation conditions. Fuel 181, 34–45.
Waples, D.W., 1994. Modeling of Sedimentary Basins and Petroleum Systems. In: Magoon, L.B., Dow, W.G. (Eds.), The petroleum system from source to trap: AAPG Memoir, 60, pp. 307–322.
Connan, J., 1984. Biodegradation of crude oils in reservoirs. In: Brooks, J., Welte, D.H. (Eds.), Advances in Petroleum Geochemistry. Academic Press, London, pp. 299–330.
Shanmugam, G., 1985. Significance of coniferous rain frost and related organic matter in generating commercial quantities of oil, Gippsland basin, Australia. AAPG Bull. 69, 1241–1254.
Huang, W.Y., Meinschein, W.G., 1979. Sterols as ecological indicators. Geochim. Cosmochim. Acta 43, 739–745.
Shalaby, M.R., Hakimi, M.H., Abdullah, W.H., 2012. Geochemical characterization of solid bitumen (migrabitumen) in the Jurassic sandstone reservoir of the Tut Field, Shushan Basin, northern Western Desert of Egypt. Int. J. Coal Geol. 100, 26–39.

Further reading

Philp, R.P., 1985. Biological markers in fossil fuel production. Mass Spectrom. Rev. 4, 1–54.